

SOFTWARE FOR DESIGNING CUSTOM ORBITAL-CRANIOFACIAL IMPLANT PLANS

by

AMANI IBRAHIM

A thesis submitted to the
School of Computing
in conformity with the requirements for
the degree of Master of Science

Queen's University
Kingston, Ontario, Canada
December, 2016

Copyright © Amani Ibrahim, 2016

Abstract

Purpose: Custom crano-orbital implants have been shown to achieve better performance than their hand-shaped counterparts by restoring skull anatomy more accurately and by reducing surgery time. Designing a custom implant involves reconstructing a model of the patient's skull using their computed tomography (CT) scan. The healthy side of the skull model, contralateral to the damaged region, can then be used to design an implant plan. Designing implants for areas of thin bone, such as the orbits, is challenging due to poor CT resolution of fine structures. This makes preoperative design time-intensive since thin bone structures in CT data must be manually segmented. The objective of this thesis was to research methods to accurately and efficiently design crano-orbital implant plans, with a focus on the orbits, and to develop software that integrates these methods. **Methods:** The software consists of modules that use image and surface restoration approaches to enhance both the quality of CT data and the reconstructed model. It enables users to input CT data, and use tools to output a skull model with restored anatomy. The skull model can then be used to design the implant plan. The software was designed using 3D Slicer, an open-source medical visualization platform. It was tested on CT data from thirteen patients. **Results:** The average time it took to create a skull model with restored anatomy using our software was $0.33 \text{ hours} \pm 0.04 \text{ STD}$. In comparison,

the design time of the manual segmentation method took between 3 and 6 hours. To assess the structural accuracy of the reconstructed models, CT data from the thirteen patients was used to compare the models created using our software with those using the manual method. When registering the skull models together, the difference between each set of skulls was found to be $0.4 \text{ mm} \pm 0.16 \text{ STD}$. **Conclusions:** We have developed a software to design custom cranio-orbital implant plans, with a focus on thin bone structures. The method described decreases design time, and is of similar accuracy to the manual method.

Statement of Co-Authorship

The work presented in this thesis was accomplished under the supervision of Dr. Gabor Fichtinger. The software was developed in collaboration with Dr. Michael Hardisty. Dr. Gabor Fichtinger and Dr. Michael Hardisty both provided feedback and corrections to the manuscript. Dr. Andras Lasso provided additional supervision, development recommendations, as well as feedback with regards to code development.

Most of the work presented in this thesis has been previously presented at the 14th Imaging Network Ontario Symposium. (A. Ibrahim, M. Hardisty, A. Lasso, G. Fichtinger, J. Mainprize, C. Whyne, “Image Processing Software for Designing Custom Craniofacial Implants”, ImNO 2016 Proceedings, presented Mar 31, 2016).

Acknowledgments

First and foremost, I would like to thank Dr. Gabor Fichtinger for his immeasurable guidance and motivation. Professor Fichtinger, I cannot begin to express how grateful I am for your support and encouragement over these years. Thank you for welcoming me into the Perk Lab, and for providing me with so many fulfilling opportunities. Thank you for immersing our lab in your contagious enthusiasm. Thank you for constantly pushing me to achieve greater success. Thank you for believing in me. Thank you for your kindness. I could not have asked for a better mentor.

I would like to thank Dr. Michael Hardisty for his continued support and collaboration on this project. Michael, it has been so much fun working with you. Thank you for giving me the space to explore. I appreciate all the direction, feedback, and support you have provided on this project. Also, thank you for being the perfect complement in software development and liking C++ more than me.

I would like to thank Dr. Andras Lasso for guiding the project's software architecture, and for being a constant intellectual resource. Andras, you have made me a better programmer and a better researcher. Thank you for always finding the time to answer my endless list of questions, and for always being ready to help. I would still be using Slicer 4.3 if it were not for you.

I would like to thank Dr. Cari Whyne for her support, and for giving me the opportunity to collaborate with the OBL team. Cari, thank you for immediately making me feel welcome when I first joined your group. I truly appreciate the opportunity you have given me to work with you and your talented team of researchers.

I would like to thank James Mainprize, Oleh Antonyshyn, and Glenn Edwards of the Calavera team for taking me on as a collaborator on this project. James, Oleh, and Glenn, thank you, it has been very rewarding being part of this work. I would like to acknowledge that my research has been funded by FedDev Ontario.

I would like to thank the members of the Perk Lab for making up what I know to be the Perk Lab. You are all such inspiring people. You have filled our research space with creativity and warmth. Thank you for the sushi lunches and the tea “parties”. Thank you for making me part of your family.

I would like to thank the members of the OBL for creating such a fun and enriching research environment. It has been so wonderful sharing a space with you. You make my commute to Sunnybrook seem exciting because I know that when I arrive, I can spend time with all of you.

I would like to thank Irene LaFleche for all of her academic and emotional support. Irene, your encouragement and kindness has meant the world to me. Thank you for always being there to listen, to help, and to make me smile.

I would like to thank my family and friends for keeping me grounded. Thank you for a lifetime of support, and for fostering my happiness.

Glossary

3D 3 Dimensions/Dimensional.

CAD Computer-Aided Design.

CLI Command Line Interface.

CT Computed Tomography.

GUI Graphical User Interface.

ICP Iterative Closest Point.

ITK Insight Segmentation and Registration Toolkit.

NLopt Nonlinear Optimization.

PSF Point Spread Function.

UIQI Universal Image Quality Index.

VTK Visualization Toolkit.

Contents

Abstract	i
Statement of Co-Authorship	iii
Acknowledgments	iv
Glossary	vi
Contents	vii
List of Figures	viii
List of Tables	ix
Chapter 1: Introduction	1
1.1 Motivation	3
1.2 Thesis Objectives	4
1.3 Thesis Outline	5
Chapter 2: Background	7
2.1 Custom Craniofacial Implants	7
2.2 Image Processing for the Craniofacial Skeleton	10
2.3 Image Restoration of the Craniofacial Skeleton	10
2.4 Surface Creation and Restoration of the Craniofacial Skeleton	15
Chapter 3: Methods	19
3.1 Development Outline	19
3.2 Software Implementation	25
3.2.1 Enhance Volume	26
3.2.2 Make Model & Fill Holes	34
3.2.3 Create Plan	39
3.3 Software Application Study	43

Chapter 4: Results and Discussion	47
4.1 Results	47
4.2 Discussion	52
Chapter 5: Conclusions and Future Work	53
5.1 Conclusions	53
5.2 Future Work	53
Bibliography	55
Appendix A:	59

List of Figures

1.1	: (a) Titanium mesh being cut and (b) hand-shaped, a process conventionally carried out intra-operatively [5].	2
1.2	(a) Titanium implant shaped using custom mould of left orbital floor; (b) Insertion of implant below left orbital floor [13]. (Permission granted for use.)	3
1.3	(a) Patient CT data, where areas of thin bone, including the orbit (red circle), are difficult to resolve and segment; (b) Reconstruction of the CT, where the patient's healthy orbit (red circle) appears damaged due to faulty bone segmentation.	5
2.1	(a) Patient with a cranial defect; (b) Model of skull defect and custom cranial implant; (c) Patient after implant insertion [7]. (Permission granted for use.)	8
2.2	(a) Axial slice from the zygomatic bone in the original CT scan; (b) Resulting CT scan after 80 iterations of deblurring; c) The registered μ CT scan; (d-f) The associated segmented cortical models of 'a', 'b', and 'c', respectively, thresholded at 1200 HU [18]. (Permission granted for use.)	12

2.3	(a) Intensity profile along the posterior maxillary sinus wall of a CT image, where there is a three-layer structure of air, bone, and tissue; (b) Profile from the posterior maxillary sinus wall is represented by $n = 3$, according to $B(x) = Y * G$ (black plots). The true intensity and geometry of the nonblurred layers are also shown (grey plots) [19]. (Permission granted for use.)	14
2.4	Fandisk and Moai models, which are frequently used to check the results of the denoising algorithms. (a) Fandisk model with noise 0.2; (b) Denoised Fandisk model; (c) Moai model with unknown noise; (d) Denoised Moai model. [3]. (Permission granted for use.)	17
3.1	(a) Original CT, where red box highlights blurry thin bone structures; (b) CT after Richardson-Lucy Deconvolution, where red box highlights restored thin bone structures; (c) CT after unsharp masking, where red box highlights sharpened thin bone structures.	21
3.2	(a) Original binary volume; (b) Binary volume after enforcing spherical topology.	22
3.3	Load Volume module: (a) Volume was loaded in scene; (b) DICOM Browser view.	27

3.4 Estimate PSF module: (a) Initial state of module; (b) Rulers were placed in the scene, and the intensities associated with the highlighted green ruler can be seen plotted in the quantitative scene view (top-right quadrant); (c) The In-Plane PSF was estimated, generating two new plots in the quantitative view (where the blue plot displays the predicted intensities and the green plot displays the estimated PSF convolved with the predicted intensities).	30
3.5 Sharpen Volume module: (a) An ROI was placed around the desired regions to sharpen: the orbital and sinal cavity; (b) The volume was clipped down to the ROI; (c) Richardson-Lucy Deconvolution was selected as the sharpening method; (d) The sharpened ROI was merged with the remainder of the original volume.	33
3.6 Save Deblurred Volume module: The sharpened volume exported to a local directory with the input volume's metadata.	34
3.7 Make Label & Convert to Model module: (a) A label was created for the volume; (b) The volume was thresholded, populating the label (green); (c) Post-process was checked to apply the spherical topology enforcing filter to the label, and then a model was reconstructed using the label.	36
3.8 Smooth Model module: The model was smoothed using the two-step smoothing filter.	37
3.9 Fill Holes in Model module: (a) Hole-filling piece was initialized; (b) Fiducial points were placed around hole; (c) Hole-filling piece was created, and fiducial points were hidden by ticking appropriate checkbox.	39

3.10 (a) Clone Model & Register module: (a) Create ICP Registered Plan button was pressed, creating a mirrored, registered model (green) of the original (grey); (b) The geometry of both models was merged and used to create a new model (white).	41
3.11 Clip Plan module: (a) An ROI encapsulates the selected model; (b) The model was clipped to the desired area by resizing the ROI.	42
3.12 (a) Segmented undamaged region of the right orbit (blue) and segmented implant (green); (b) Skull model in which the right undamaged region was registered to the left undamaged region, and the implant from the right orbit was registered to the healthy surface of the left orbit.	45
3.13 (a) Segmented surface model of the healthy orbit created using our software; (b) Skull model created using Calavera Surgical's™ existing methods overlaid by the segmented surface model created using our software.	46
4.1 Post-operative patient skull models displaying distance between implant model and contralateral healthy orbit, where the implant was designed by (a) Calavera Surgical's™ existing methods and (b) hand-shaping; (c) Distance colour-map.	48
4.2 (a) Undamaged orbit model of patient generated using our software (blue) against skull model generated using Calavera Surgical's™ current method; (b) Distance colour-map.	49

List of Tables

4.1	Morphological Analysis: Implant vs Contralateral Orbit	50
4.2	Morphological Analysis: Implant vs Contralateral Orbit (Statistics) .	50
4.3	Morphological Analysis: Design Using Our Software	51
4.4	Morphological Analysis: Design Using Our Software (Statistics) . . .	51

Chapter 1

Introduction

Craniofacial defects are deformities in the region of the skull caused by congenital abnormalities, trauma, tumours, and other disease [12]. Severe craniofacial defects often compromise aesthetics and function of the craniofacial skeleton, and require reconstructive surgery.

Craniofacial implants are used to restore the cranial and facial skeletal anatomy which has been compromised. Conventionally, implants are formed by hand-shaping and clipping titanium mesh sheets (Figure 1.1) in the operating room during the reconstruction surgery [22]. When the surgeon is satisfied with the shape and fit of the implant, it is secured over the defected area. Using hand-shaped implants for reconstruction of the craniofacial skeleton presents specific challenges for reconstructive surgical techniques due to the skull's complex anatomy and the uniqueness of each patient's defect [20].

Custom craniofacial implants are designed to fit a patient's specific defected anatomy. Their design is carried out pre-operatively by a specialized medical technician. Computed tomography (CT) scans are used to determine the patient's skull geometry. CT is the primary modality used to capture bone data because of the

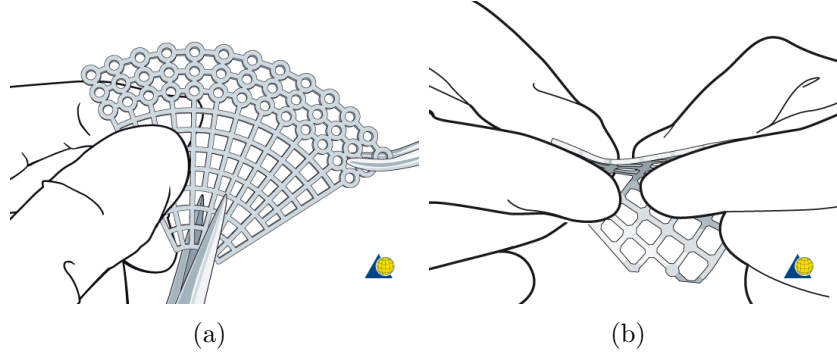


Figure 1.1: : (a) Titanium mesh being cut and (b) hand-shaped, a process conventionally carried out intra-operatively [5].

strong contrast of bone in X-ray imaging compared against soft tissue and air [18].

After the technician has obtained a patient’s CT data, computer-aided design (CAD) software is used to create a custom implant design. The technician from Calavera SurgicalTM, our commercial partner on this project, uses CAD software to first generate a three-dimensional (3D) model of the patient’s skull using that patient’s CT scan. An implant plan is then designed for the defected skull region. This is done by mirroring the anatomy of the contralateral, healthy side of the skull model, and using it as a guide to reconstruct the defected region. A custom mould is then milled using the plan, where the mould is used in the operating room to deform the titanium mesh sheet into the desired implant geometry. The mesh sheet is pressed into the mould, causing it to bend into the correct anatomical shape. (Figure 1.2(a)).

The use of CAD craniofacial implants has advantages over their hand-shaped counterparts [20]. Using CAD implants can yield a better fit, which leads to better cosmetic and functional outputs. Additionally, pre-operative design leads to reduced surgical time which can reduce patient discomfort and risk of infection.

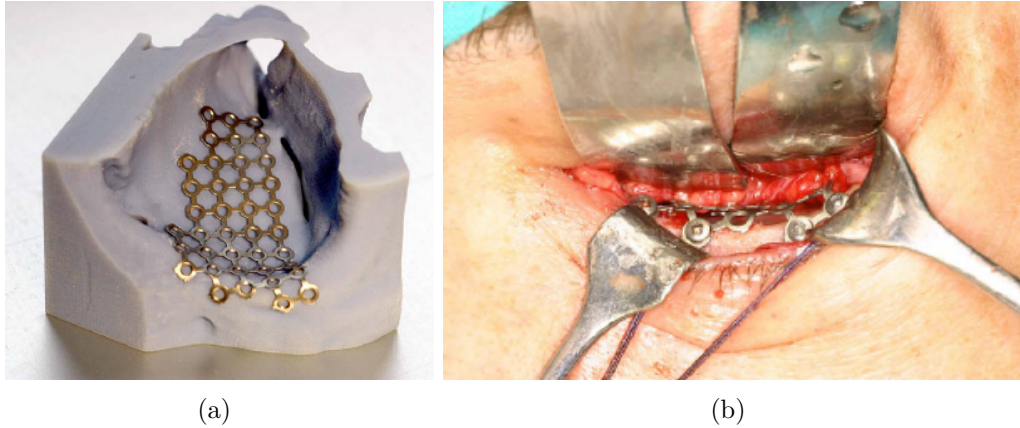


Figure 1.2: (a) Titanium implant shaped using custom mould of left orbital floor; (b) Insertion of implant below left orbital floor [13]. (Permission granted for use.)

1.1 Motivation

The pre-operative design of custom implants takes 1 to 6 hours of expert engineering time [17]. The amount of time required varies with the complexity and location of the defected structure. Thin bone structures present a particularly difficult design problem. Difficulties arise due to the limited ability to resolve thin bone structures using clinical CT. Poorly-resolved thin structures lead to skull models that have incorrect topology or holes. This renders the models unusable for plan generation. To remedy the inaccuracies in these cases, CT scans are re-processed. Each CT slice of the target area is visually examined, and thin bone that has not been accurately segmented is manually corrected. The examination and corrections can make the generation of an accurate skull model very time-consuming.

The orbit is the bony socket in which the eyeball rests. During imaging, the orbit is one of the primary thin bone structures detrimentally affected by CT image resolution [18]. Bony orbital regions in a CT scan appear blurry and have degraded

intensity, causing the reconstructed skull model to appear to have two defected orbits (Figure 1.3). The orbital bone structures in the CT scan are manually segmented, ultimately making custom implant design for orbital fractures impractically time-consuming.

Orbital fractures are the most common injury to the face, making up 40% of maxillofacial traumas, and causing asymmetry of the orbits [13]. Asymmetry of the orbits creates both a cosmetic and a functional problem. Diplopia is a common side-effect of orbital asymmetry. It causes afflicted patients to lose the ability to resolve images clearly. Cosmetically, orbital fractures can give eyes a sunken appearance.

Surgical repair of orbital fractures is especially challenging because of the complexity and lack of visibility during surgery. These factors make it particularly challenging to create well-fitting, hand-shaped implants, and highlight the benefits of CAD implants. An internal report from Calavera SurgicalTM states that using CAD orbital implants reduces surgical time by a factor of three, and reduces the risk of requiring further reconstruction operations due to poor-fitting implants [17]. CAD implants have seen increased adoption; however, significant challenges still exist in the design phase of implant creation.

1.2 Thesis Objectives

The goal of this master's thesis is to create software for the time-efficient and accurate design of custom craniofacial implant plans, with a focus on the orbits. Implant plans are designed to restore symmetry to the craniofacial skeleton, and their ability to do so relies on using anatomically-accurate skull model reconstructions. Therefore, our software should provide image processing tools for quickly and accurately restoring the

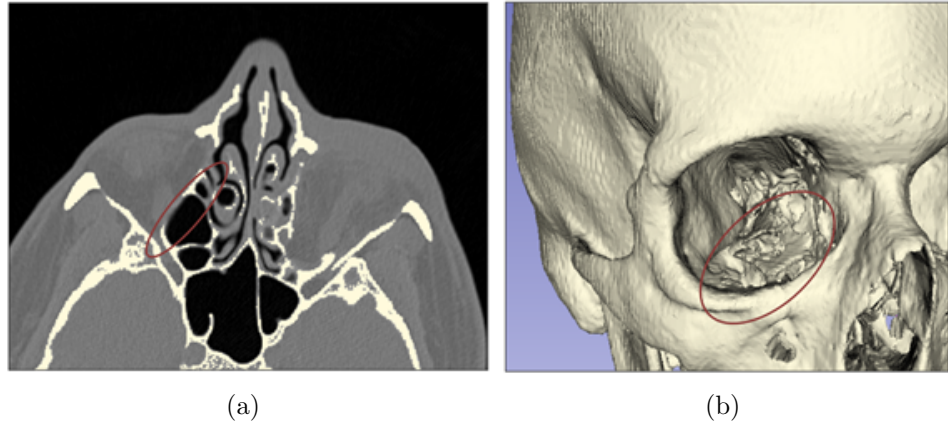


Figure 1.3: (a) Patient CT data, where areas of thin bone, including the orbit (red circle), are difficult to resolve and segment; (b) Reconstruction of the CT, where the patient’s healthy orbit (red circle) appears damaged due to faulty bone segmentation.

correct geometry to bone structures in both the CT data as well as the corresponding skull models reconstructed from that data. The skull models that are generated using our software should closely match the geometry of the skull models generated using the current manual method utilized by Calavera SurgicalTM, while significantly decreasing the overall design time. Our software should also provide surface manipulation tools for using these skull models to ultimately design implant plans. The software tools should focus on the design of orbital implant plans since their current production process is particularly inefficient. However, the tools should also be applicable to the generation of craniofacial implant plans in general.

1.3 Thesis Outline

This thesis is divided into five chapters. Within the chapters, I present the advantages of custom orbital-craniofacial implants, the current difficulties with designing such implants, methods for overcoming these difficulties, and software that has been

developed to incorporate the methods. The thesis goes on to demonstrate the success of the software by reviewing its application to patient data, and presenting an analysis of those results. The thesis is organized as follows:

Chapter 2, Background: This section provides a literature review on custom craniofacial implants, and discusses topics related to the design of craniofacial implants, including image acquisition, medical image processing, and surface quality processing.

Chapter 3, Methods: This section details the tools and methods used in creating our software. It provides a detailed walk-through of each module in the software workflow. The section closes by discussing how the software has been applied to patient data and tested for accuracy.

Chapter 4, Results and Discussion: This section presents the results of comparing designs created by our software to the existing CAD methods, as well as analyzing how well CAD implants reproduced shape and symmetry against those hand-shaped.

Chapter 5, Conclusions and Future Work: This section revisits the problems associated with designing custom craniofacial implants, and goes over the methods incorporated in our software that were used to tackle them. It goes on to review the findings that can be drawn from the application of this software.

Chapter 2

Background

Open reduction and internal fixation of facial fractures became popular in the 1970s and 80s, and they remain the standard of care for most facial fractures [21]. The goal of these surgeries is both functional and cosmetic, and often involves restoring symmetry that has been disrupted by defects. However, the accurate restoration of complex craniofacial structures can be extremely difficult. The most challenging cases include defects in the orbits, naso-orbito-ethmoid, and zygomaticomaxillary complexes [21].

2.1 Custom Craniofacial Implants

In recent years, presurgical planning has been conducted with computer-aided design (CAD) software, making the treatment of complex injuries more successful [20]. Using CAD tools and patient-specific CT data, a three-dimensional (3D) model of the patient's skull can be successfully reconstructed. There are several cases in which an accurate skull model assists surgeons in recognizing the defected areas of the skull, creating a plan of treatment, and predicting surgical outcomes [14, 20].

There are many advantages to using CAD tools for the design of the custom

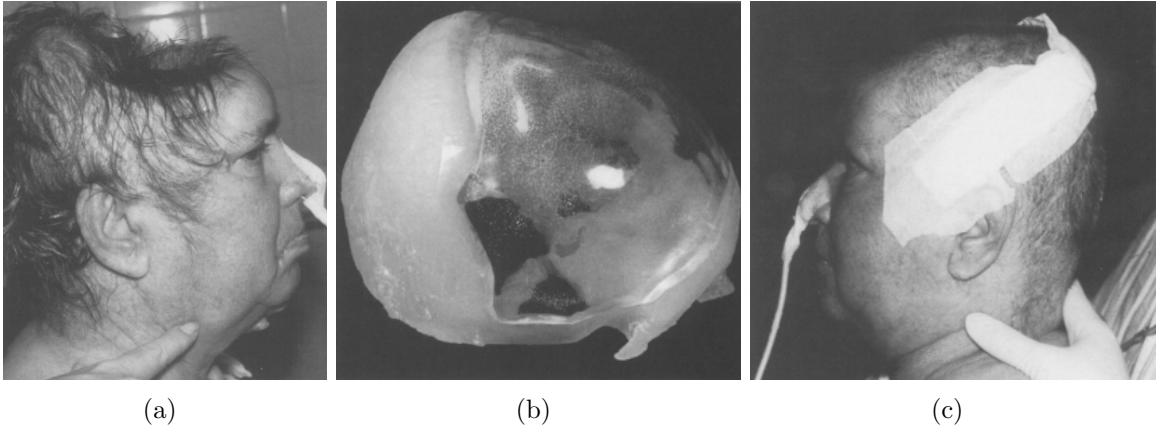


Figure 2.1: (a) Patient with a cranial defect; (b) Model of skull defect and custom cranial implant; (c) Patient after implant insertion [7]. (Permission granted for use.)

implants. Compared to the standard of care, the customisation and prefabrication of implants have been shown to reduce operating time, improve cosmetic outcome, and lead to fewer complications [7, 23]. A number of studies exist in the literature that show these positive outcomes.

One study discussed the results of treating thirty patients requiring cranioplasties with customised cranioplastic implants [7]. Patient-specific CT data was used to create a model of each patient's skull. Imaging techniques of mirroring and interpolating were applied to the models to extend the existing anatomy, and to ultimately design so called "master implants" to fit the defected areas of the skull models. The master implants were used to create cavity moulds which were then used to cast custom acrylic implants (Figure 2.1). The surgeons who treated patients using these custom implants reported reduced operating time and a greatly improved cosmesis outcome [7]. The patients also felt positively about the integration of CAD tools. They reported that their understanding of the procedure was improved because they were able to see a model of their skull defect and implant, preoperatively [7].

Another study reported on the results of applying custom-fabricated chin augmentation implants to three patients [23]. Patient CT data and CAD tools were used to create a master implant for each patient, for use in restoring structure to that patient's specific facial fracture. The master implant was used in the production of a mould, which was then used to cast the titanium implant. This approach showed significant advances to traditional methods. The intra-operative fit of the implant was better, the operating time was reduced, and there was a positive aesthetic outcome post-surgery. Over the mean follow-up period of 1.5 years, the aesthetic of the implant remained excellent and no complications emerged.

It is clear that CAD tools are beneficial to the restoration of symmetry to facial skeletal structures. Such tools are especially important in cases of complex and hidden anatomy, such as the orbits. One study focusing on orbital reconstruction looked at 29 patients with posttraumatic enophthalmos. Enophthalmos is the backward and downward displacement of the eyeball in the orbit. In the study, 24 of the 29 patients were also experiencing diplopia [15]. Using CT data, custom titanium implants were designed and inserted in the damaged orbits. As a result, enophthalmos was treated successfully in 29 (100%) patients, and diplopia was improved or cured in 14 (50%) patients. The study states that the use of pre-formed implants significantly reduced operation time since it decreased trial-fitting and soft tissue manipulation; however, it also states that a primary limitation in creating the custom implants was production time. Anecdotally, similar results were reported by Calavera Surgical™. Surgery times were reduced by a factor of three upon using custom implants, but they were paired with a high design production time-range of 3 to 6 hours. None of these studies quantified implant and placement accuracy. Instead, they assessed clinical outcome

2.2. IMAGE PROCESSING FOR THE CRANIOFACIAL SKELETON

variables.

2.2 Image Processing for the Craniofacial Skeleton

Data acquisition of the craniofacial skeleton is generally carried out by CT scanning. CT is susceptible to scanning artifacts. The point spread function (PSF) characterizes the response of an imaging system (e.g., CT machine) to an object [6]. Specifically, the PSF of a CT describes the blurring due to X-ray scattering and limitations caused by the scanner's focal spot and detector response [6]. In general, imaging systems can be represented by the equation: $f = Kf_{true} + \epsilon$, where the true image, f_{true} , is convolved with the PSF, K , and corrupted by some level of error due to noise, ϵ . The PSF determines the size of the smallest structures that may be resolved by an imaging system. The bones around the orbital and sinal regions are the thinnest bones in the human body, with a thickness of 0.4-1.5 mm [18]. The resolution of clinical CT machines is typically 0.4-1 mm, resulting in such structures being susceptible to a blurring effect [11]. The primary result on such bone structures is that their thickness is overestimated and their density is underestimated. When CAD software is used to reconstruct a skull model from CT data, the fine-structured areas affected by the PSF will not be translated correctly.

2.3 Image Restoration of the Craniofacial Skeleton

Enhancement in the ability to resolve fine structures in microscopy and clinical CT machines has been extensively studied in the literature [8, 18, 24].

Unsharp masking is a technique that has been used to edge-enhance CT scans [8]. The algorithm begins by creating a blurred negative image of the original. The

2.3. IMAGE RESTORATION OF THE CRANIOFACIAL SKELETON

blurred negative is then combined with the original to create an image that is sharper than the original. This algorithm can be represented by $\text{sharpened} = \text{original} + (\text{original} - \text{blurred}) * \text{amount}$, where sharpened is the enhanced image, original is the original image, blurred is the original image convolved by a Gaussian mask, and amount is some weighing factor. The effect of unsharp masking relies on the size of the mask and the weighing factor. The size of the mask affects the size of the edges to be enhanced, where a smaller mask enhances smaller-scale detail. The weighing factor controls what percentage of the blurred negative is added to the original image. By modifying this, the level of sharpness and contrast added at the edges can be varied. In one study that evaluated the use of unsharp masking on five clinical fracture cases, the optimal combination of mask size and weighting factor was 3x3 pixels and 5, respectively, as it produced the best resolution outcome, assessed by visual inspection. Image restoration using unsharp masking has little computational expensive and does not require the imaging system's PSF to be known.

Another method which has been used to sharpen CT data successfully is Richardson-Lucy Deconvolution [1, 18]. Richardson-Lucy Deconvolution is part of a larger class of iterative deconvolution algorithms which attempt to recover an uncorrupted image from that obtained through an imaging system. Iterative deconvolution is necessary since directly deblurring an image may increase its levels of noise, further corrupting it. The Richardson-Lucy Deconvolution algorithm uses an iterative scheme that relies on expectation-maximization to get closer to an estimate of f_{true} . Richardson-Lucy Deconvolution requires knowledge of the image's PSF either by measurement or estimation. While f_{true} cannot be perfectly recovered, a closer similarity to f_{true} is possible than the observed f [18, 25].

2.3. IMAGE RESTORATION OF THE CRANIOFACIAL SKELETON

In a study conducted by Pakdel *et al.* that focused on thin bone structures, the results of deblurring CT images of a cadaveric sample with Richardson-Lucy were observed [18]. The resulting CT scans and the reconstructed 3D models were compared with a high-resolution micro-CT (μ CT) of the same sample, as a reference (Figure 2.2). μ CT scanners image small-scale objects, but with very high resolution, making them useful for generating true representations of small structures. The optimal number of iterations for restoring geometry to CT data was determined to be 80 since it resulted in the highest reduction in thickness and intensity error, while minimizing the increase in intensity variance. The corresponding deblurred CT scan had an overall mean cortical thickness error reduction of 3.8 ± 1.5 mm, where the mean thickness of the μ CT reference volume was 1.08 ± 0.77 mm. This resulted in greatly improved topology of thin bone regions.

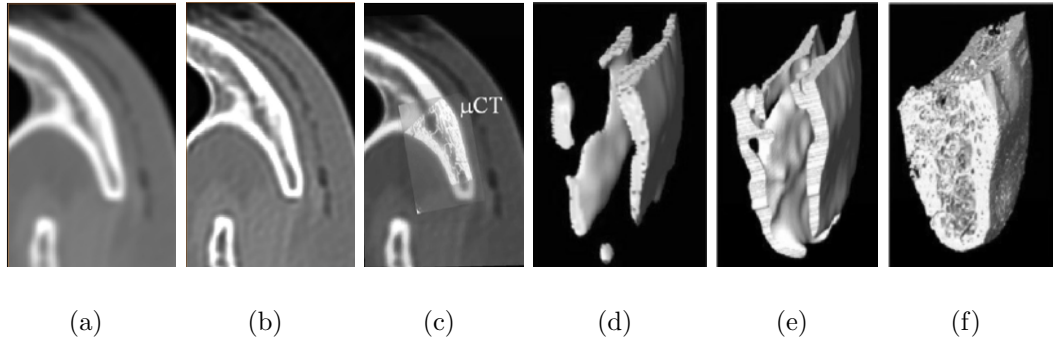


Figure 2.2: (a) Axial slice from the zygomatic bone in the original CT scan; (b) Resulting CT scan after 80 iterations of deblurring; c) The registered μ CT scan; (d-f) The associated segmented cortical models of 'a', 'b', and 'c', respectively, thresholded at 1200 HU [18]. (Permission granted for use.)

In another study, a series of CT images were corrupted with Gaussian blur, and Richardson-Lucy Deconvolution was used in an attempt to recover the images [1].

2.3. IMAGE RESTORATION OF THE CRANIOFACIAL SKELETON

The average accuracy of the recovery was calculated using the universal image quality index (UIQI). The UIQI is measured by looking at a combination of three factors: loss of correlation, luminance distortion, and contrast distortion. Each factor is given a value between 0 and 1, subtracted from 1, and then multiplied to determine the final index value which can have a value in the interval of [-1 to 1] [27]. A UIQI value near to 1 represents a good quality image. The images recovered using Richardson-Lucy were found to have a value of 0.8348, where the degraded images had an average UIQI of 0.7854. This improvement difference was found to be qualitatively noticeable.

To apply Richardson-Lucy Deconvolution, the PSF must be known. Since the CT images were intentionally blurred in the aforementioned study, the PSF could be directly calculated, and did not need to be estimated. However, in the study conducted by Pakdel *et al.*, and in practical cases, blurring was due to CT image acquisition. The PSF is variable for different CT scans, as it is specific to the manufacturer of the machine, scanning parameters, and reconstruction of the scan. Users do not have access to the PSF information of a given scan, and therefore, the PSF must be estimated or measured.

Pakdel and Treece present two very similar methods for estimating the PSF [19, 26]. The PSF was estimated by first locating fine bone structures within the scan, whereby a three-layer structure was observed, and profiles were drawn across them (Figure 2.3(a)). The intensities (X) along the profile were then plotted. The PSF was assumed to be an orthotropic Gaussian (G). The PSF was then estimated by fitting the resulting image profile intensities (B) with the function of the three-layer model (Y) (representing the true intensity and geometry of the non-blurred layers) convolved with the estimate of the PSF, $B(x) = Y * G$ [19]. The estimated PSF

2.3. IMAGE RESTORATION OF THE CRANIOFACIAL SKELETON 4

was then used to deblur the image volume with the Richardson-Lucy Deconvolution algorithm.

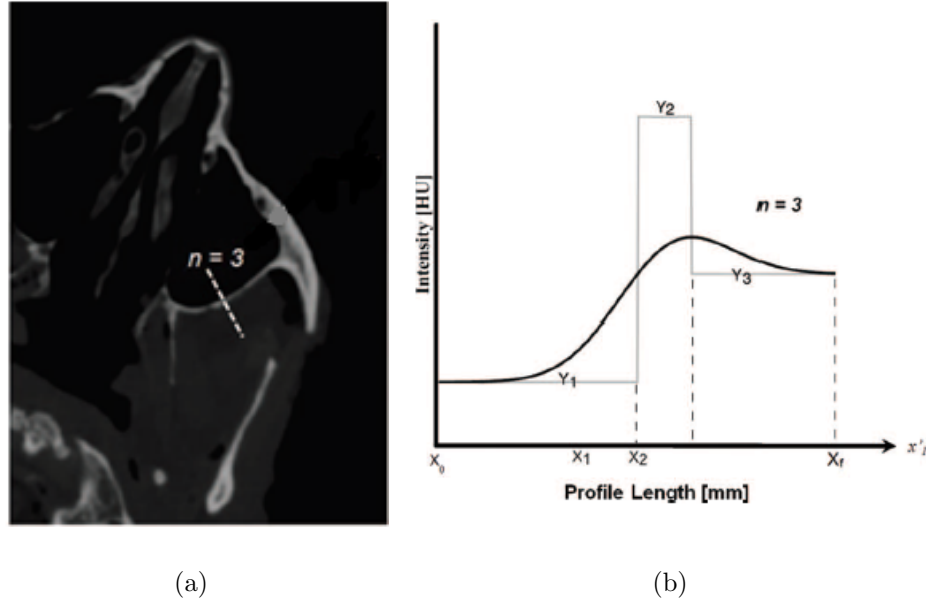


Figure 2.3: (a) Intensity profile along the posterior maxillary sinus wall of a CT image, where there is a three-layer structure of air, bone, and tissue; (b) Profile from the posterior maxillary sinus wall is represented by $n = 3$, according to $B(x) = Y * G$ (black plots). The true intensity and geometry of the nonblurred layers are also shown (grey plots) [19]. (Permission granted for use.)

Structural information may also be restored to the skull after bone has been segmented from CT data. A filter developed by Styner *et al.* enforces a binary volume to have spherical topology [24]. This means that all cavities completely enclosed within the segmentation are filled. The filter uses two operations to carry this out: first, it applies a binary closing operation, and then it applies a level set based anti-alias smoothing operation.

2.4 Surface Creation and Restoration of the Craniofacial Skeleton

Given a binary CT volume, there exist several reconstruction algorithms to generate a surface model, and restoration algorithms that can be used to reduce noise and close holes in that surface.

One method of converting voxel data to a surface model is the marching cubes algorithm [16]. Marching cubes goes through the volume, and creates imaginary cubes from 8 adjacent voxel values. A threshold value is used to relabel the cube vertices as being inside or outside the surface. The binary pattern of the vertices is matched against a pre-defined list of 256 (2^8) patterns and the corresponding triangles they form within the cube. These polygons are used to generate the final model. The marching cubes algorithm is easy to parallelize since cells are processed independently. This makes it ideal for the generation of large volumes.

A method of converting point data to a surface model, directly, is 3D Delaunay triangulation. Given a set of points, Delaunay triangulation creates a convex hull that has the property that the circumsphere of any tetrahedron contains no other points of the point set, P , except the 4 defining points of the tetrahedron. (This property translates to n dimensions.) The result is a surface that avoids narrow triangles since they have large circumspheres compared to their area. There are different algorithms that can be followed for creating 3D Delaunay triangulations. Watson and Bowyer propose one such technique [4]. It begins by bounding P , the bounding triangulation. Each point of P is then injected into the triangulation. If an injected point lies within the circumsphere of any tetrahedron, then that tetrahedron is deleted. This leaves holes in the triangulation. In the next phase, the two-dimensional faces on the boundary of the holes, and the corresponding rejected injected points, are used to create

an updated triangulation. During the final phase, the tetrahedra that connected the points forming the initial bounding triangulation are removed. This completed the Delaunay triangulation.

A surface reconstructed from point data can be noisy and jagged. Common techniques for removing noise from surfaces are based on Laplacian and Gaussian operations [3]. While they effectively remove noise from the surface to which they are applied, they also smooth surface characteristics that should remain sharp. This causes the resultant model to be smaller and deformed.

An approach proposed by Bian *et al.* presents a two-step smoothing filter which removes noise from the surface model, while preserving features of the surface (Figure 2.4) [3]. The algorithm first classifies the vertices into two clusters, feature and non-feature, to determine which areas to smooth. This information is then used to update the vertices' positions, creating appropriate surface face normals. Then, a drag-back updating algorithm is used to push back feature cluster points to locations that are closer to their original positions. These steps are carried out iteratively until a fine steady state is achieved. This method of surface denoising also closes small holes in the model.

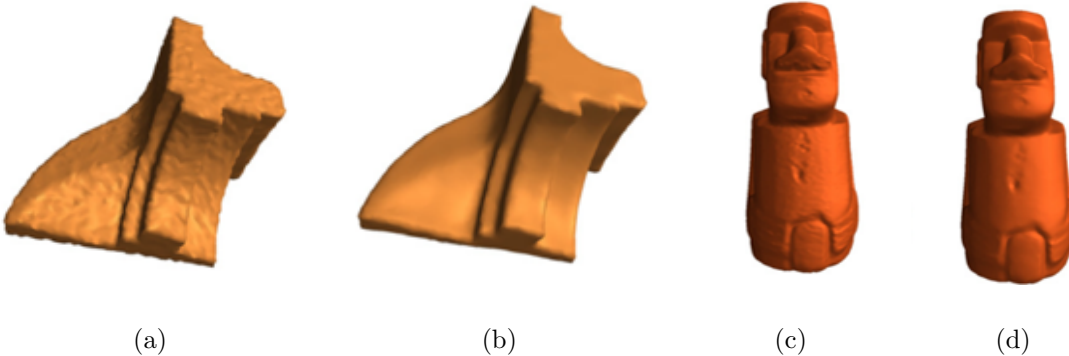


Figure 2.4: Fandisk and Moai models, which are frequently used to check the results of the denoising algorithms. (a) Fandisk model with noise 0.2; (b) Denoised Fandisk model; (c) Moai model with unknown noise; (d) Denoised Moai model. [3]. (Permission granted for use.)

Once the geometry of a surface model has been restored, it may need to be registered to another model. Surface models are simply point clouds, and there are many rigid and deformable registration techniques that can be applied to align them.

Besl *et al.* present an analysis of a popular method for the rigid registration of two point clouds, known as iterative closet point (ICP) registration [2]. ICP registration transforms one point cloud (the source) to better match the second point cloud (the reference). For each point in the source point cloud, a corresponding point in the reference cloud is found which minimizes the mean squared error cost function for the transformation needed to align the pair of points. The transformations are applied, and the algorithm is reiterated.

Jian *et al.* propose a computationally efficient method for the deformable registration of two point clouds [9]. Their algorithm successfully registers models, even in the presence of outliers and noise. Their algorithm works by modeling each set of

points using a Gaussian mixture, and registering the two mixtures based on a closed form expression for the distance between them.

The literature presents many methods for enhancing the quality of both volume and model data, as well as techniques for further manipulating it. Case studies on its application have been presented, and they provide a strong foundation on which to build.

Chapter 3

Methods

3.1 Development Outline

Our software for implant plan design was developed using 3D Slicer (www.slicer.org), a free and open-source platform used for the visualization, manipulation, and analysis of medical data. The software was designed to execute the implant planning workflow as follows:

1.
 - Task: Accept a CT volume as input.
 - Approach: The software reads the CT data, and implicitly converts it to VTK data.
 - Notes: CT data is most commonly stored as a DICOM, and 3D Slicer can accept DICOM, TIFF, JPEG, NRRD, and VTK data types as inputs. Conversion from the aforementioned file types to the VTK type makes tools from the VTK and ITK libraries available for utilization within 3D Slicer for both volume and surface model manipulations.

2.
 - Task: Enhance the quality of the CT volume.
 - Approach: The software applies Richardson-Lucy Deconvolution and unsharp masking to deblur and edge-enhance the CT volume, respectively.
 - Notes: Richardson-Lucy Deconvolution is chosen as the primary image restoration technique since it attempts to solve both the intensity under-representation and thickness over-representation problems prevalent with thin bone structures [18]. Applying Richardson-Lucy results in a restoration of both the intensity and geometry of the thin cortical structures present in the CT scans. Richardson-Lucy Deconvolution had already been implemented and available for use in the ITK library. However, the algorithm requires a volume-specific PSF value as an input parameter. Estimating the PSF of a volume is accomplished by using the method proposed by Pakdel *et al* [19]. Tools from the NLOPT library are used for optimization [10].

Unsharp masking is chosen as a secondary restoration technique since its focus is only on enhancing the appearance of an image's edges. Applying unsharp masking to CTs increases the intensity of thin bone structures, but does not fix their over-represented thickness. To implement unsharp masking, its algorithm is followed [8], and ITK filters are used for manipulating the image data (e.g., adding, multiplying, blurring it).

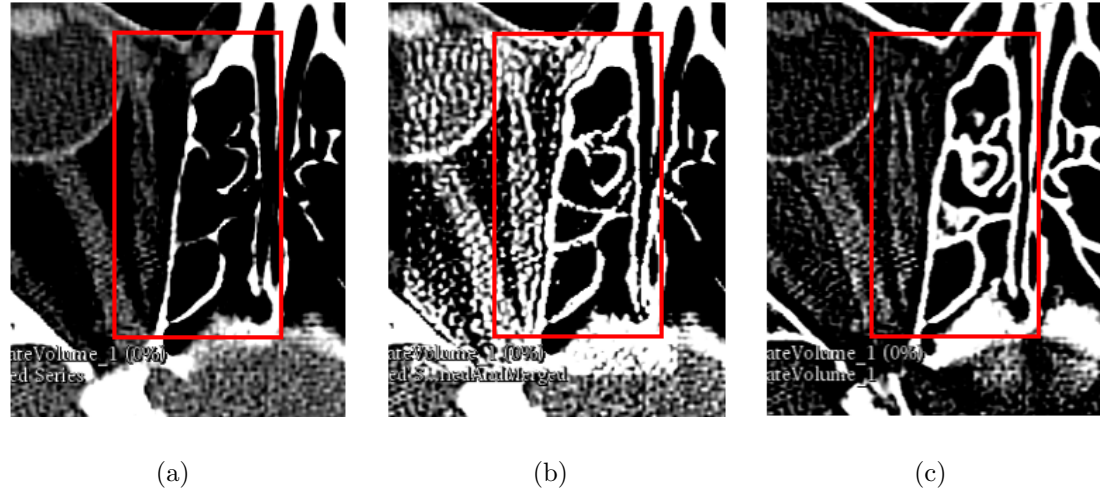


Figure 3.1: (a) Original CT, where red box highlights blurry thin bone structures; (b) CT after Richardson-Lucy Deconvolution, where red box highlights restored thin bone structures; (c) CT after unsharp masking, where red box highlights sharpened thin bone structures.

3.
 - Task: Threshold the CT volume to segment bone.
 - Approach: The software applies widgets from 3D Slicer's built-in Editor module to create a segmentation within the intensity range of bone.
 - Notes: The radiodensity of thin orbital and sinal bones begins at approximately 300 Hounsfield units (HU) and the radiodensity of cortical bone generally exceeds 3000 HU, representing the highest intensity echelon in a CT. Therefore, to capture bone, the threshold minimum for the segmentation is set to 300 HU and the threshold maximum is set to the highest intensity value present in the CT volume (which varies from scan to scan). The segmentation is stored as a binary volume.

4.
 - Task: Enhance the quality of the binary volume.
 - Approach: The software applies a filter that enforces spherical topology to increase connectivity within the binary volume.
 - Notes: Thresholding the CT volume to segment bone captures only some areas of the orbital region. If a piece is too thin, its intensity will not be high enough to be captured, leaving it to be labeled 0. This creates gaps in adjacent pixels of orbital bone in the thresholded CT slices. Since some of these gaps create internal holes in the binary volume, the filter developed by Styner *et al.* enforces spherical topology in an attempt to fill them and increase connectivity within the volume [24].

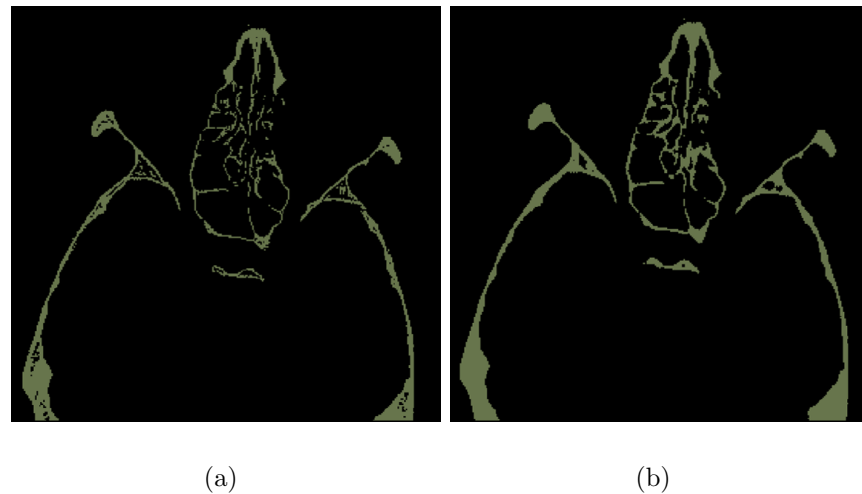


Figure 3.2: (a) Original binary volume; (b) Binary volume after enforcing spherical topology.

5.
 - Task: Convert the improved binary volume to a surface model.
 - Approach: The software uses logic from 3D Slicer's built-in Model Maker

module to reconstruct a skull model from the binary CT volume.

- Notes: The Model Maker module implements the marching cubes algorithm to generate a surface model from volume data. Marching cubes is used since its algorithm is very well-parallelized, making it a fast way to generate surfaces from volume data.

6. • Task: Enhance the quality of the surface model.

- Approach: The software applies a two-step smoothing filter to remove obvious noise from the model and close small holes present in the orbits. The software closes large holes remaining in the orbits by covering them with hole-filling surfaces generated by triangulating a set of user-placed points. The software then utilizes a deformable registration method to match the curvature of the hole-filling surfaces with the skull model.
- Notes: The application of sharpening tools at step 2 invariably adds noise to the data, and consequently, to the surface model reconstructed from the data. VCG has a two-step smoothing filter that is based on the work by Bian et al. that removes noise from the model, while preserving model characteristics [3]. This filter removes noise from the skull model, but preserves the geometry of its anatomical structures.

Large holes remaining in the orbits are filled by creating surfaces to cover the holes. A series of points are placed around each hole in the skull. Then, a VTK filter is applied to snap the points to the closest corresponding points on the skull model. Using 3D Delaunay triangulation,

which is implemented as a VTK filter, these points are used to generate a surface for each hole. Delaunay triangulation is used since it efficiently generates a convex hull, given a set of data points. This translates to fewer points being required in order to generate surfaces that fill the holes.

Although the surfaces cover the holes, there will be a clear mismatch between the curvature of the skull model and the hole-filling surfaces. To fix this, deformable registration is applied to each hole-filling surface. The deformable registration method used is based on the research by Jian *et al.* [9]. Their method successfully registers models, even in the presence of outliers – essential for this application since there can only be a direct match between the areas of the hole-filling surfaces that lay directly over the material boundaries encapsulating the holes. After this step, any remaining holes in the model are minuscule enough to be negligible, and the skull model is sufficiently restored for use in custom implant plan design.

7.
 - Task: Use the restored model to create the implant plan.
 - Approach: The software clones and mirrors the skull model. Next, the software registers the original and mirrored models using ICP registration. The user carries out manual registrations to ensure that the healthy region of the mirrored model and the damaged region of the original model line up closely. The software then merges the two models to create a new model. The user clips the new model to the desired area.
 - Notes: ICP registration runs quickly, but assumes full overlap between the points of the two surface models. The skull is fairly symmetric, and so

ICP is sufficient for the automated-phase of registration. A filter to carry out ICP registration had already been implemented in VTK.

8.
 - Task: Save and export the implant plan.
 - Approach: The software saves and exports the intermediate and final models in STL format, ready for use in other software.

3.2 Software Implementation

Software was created that integrates these steps, and enabled the user to easily carry them out. The software consists of a series of modules which are linked together using a tabbed workflow, and then packaged as a guidelet. A 3D Slicer module can take the form of a command line interface (CLI), a loadable module (written in C++), or a scripted module (written in Python). The modules that make up the tabbed workflow are of all three types. A guidelet is a type of scripted module that allows the user to hide the default 3D Slicer GUI. In the guidelet view, only the necessary modules and widgets are shown to the user, creating a less cluttered interface that is easier to navigate.

The guidelet is made up of a tabbed workflow of modules. The workflow has three primary categories: *Enhance Volume*, *Make Model & Fill Holes*, and *Create Plan*. Each category has a series of secondary tabs, where each secondary tab is a standalone module. The *Enhance Volume* category contains the modules: Load Volume, Estimate PSF, Sharpen Volume, and Save Deblurred Volume. The *Make Model & Fill Holes* category contains the modules: Make Label & Convert to Model, Smooth Model, and Fill Holes in Model. The *Create Plan* category contains the

modules: Clone Model & Register and Clip Plan.

The workflow is designed to be used by going through each tab of each category, from left to right, where each category focuses on a different area of plan creation.

3.2.1 Enhance Volume

The *Enhance Volume* category is the first of the primary categories in the workflow. It enables the user to load the desired medical data, enhance its quality around areas of thin bone, and then save that enhanced volume with the original volume's metadata.

Load Volume

The Load Volume module (Figure 3.3) allows the user to load medical data into the scene. To load DICOM data, the user selects a local directory containing the DICOM files. The user can choose to load other volume formats, specifically TIFF, NRRD, and VTK, by choosing the appropriate file. The medical data will be loaded into 3D Slicer as a scalar volume node (`vtkScalarVolumeNode`). Each `vtkScalarVolumeNode` has an ID and name with which to identify it.

If the loaded file is a DICOM, it will generally have associated metadata: information about the patient and the scan itself (e.g, patient name, date of scan, modality of scan). Upon loading the DICOM, the metadata will be stored within a dictionary where the key will be the associated scalar volume node ID. This information is used by the Save Deblurred Volume module.

The Active Volume combo box displays the most recently imported volume. This can be changed manually. The Active Volume node will cascade to the inputs of the other modules, where an input volume is to be selected.

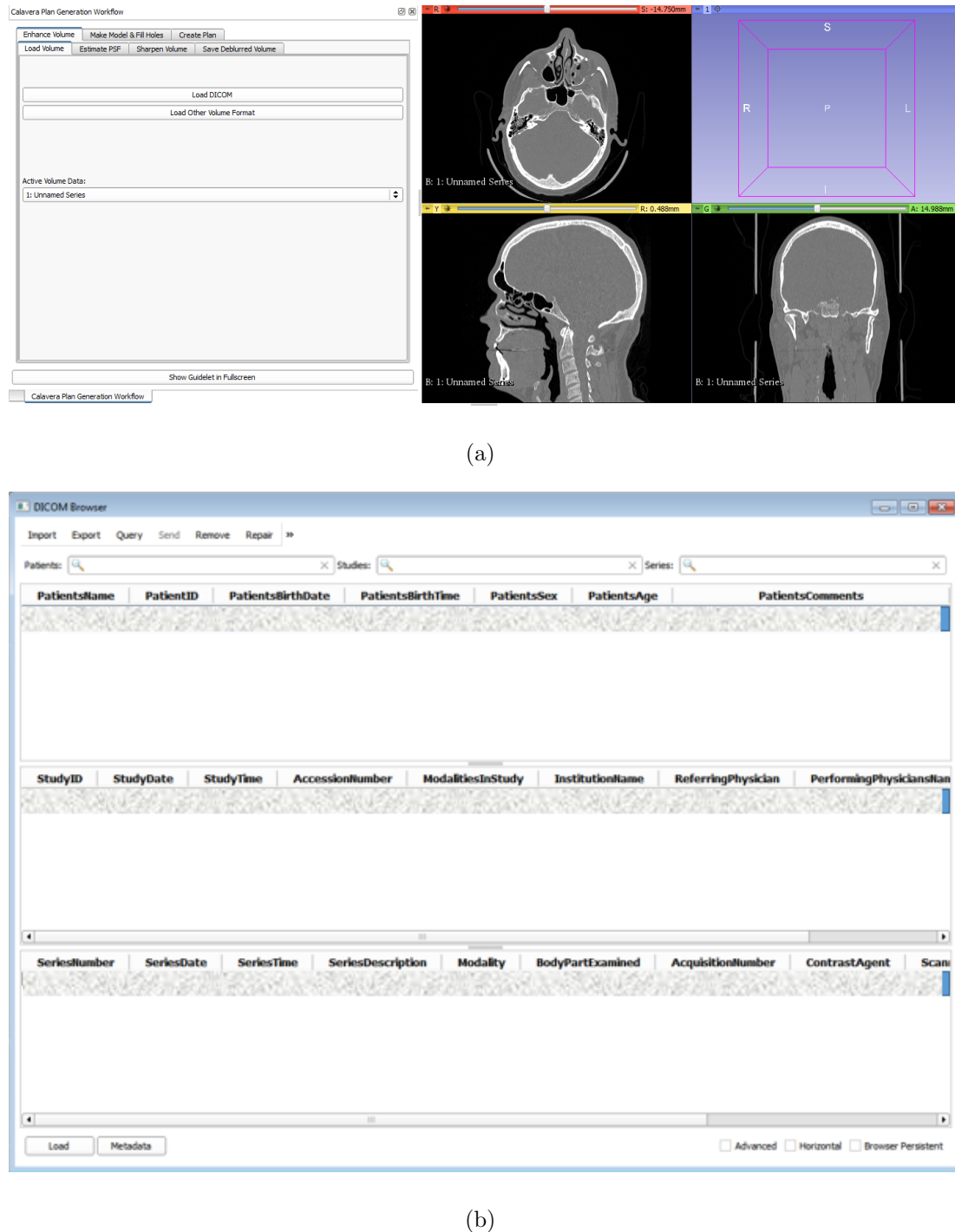


Figure 3.3: Load Volume module: (a) Volume was loaded in scene; (b) DICOM Browser view.

Estimate PSF

The Estimate PSF module (Figure 3.4) allows the user to estimate the PSF of a volume. The user begins by choosing the desired volume from a list of previously loaded volumes. The current volume defaults to the Active Volume node from the Load Volume tab.

Next, the user sets down a series of rulers over the volume data. A ruler is defined by setting down two points on a volume slice. A line segment will be drawn which connects these two points. Rulers should be drawn perpendicular to thin planar pieces of cortical bone, where the planar region does not vary greatly between adjacent slices.

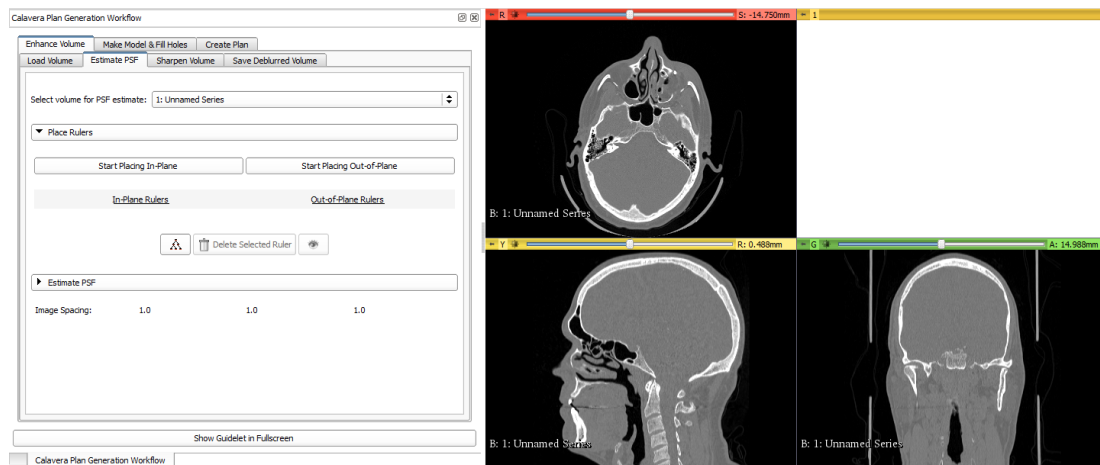
Between three and six rulers should be drawn In-Plane (the x-y direction) as well as Out-of-Plane (the x-z or y-z direction). To ensure that the rulers are drawn in the correct direction, In-Plane rulers should be placed in the red slice view quadrant, and Out-of-Plane rulers should be placed in either the yellow or green slice view quadrants. If the user has saved a set of rulers from a previous session, these may be added in the scene using the Import Rulers button.

Each ruler has a corresponding intensity profile, defined as the image intensity values lying along the ruler. Intensity profiles are plotted in the top-right slice view quadrant. This allows the user to see if the ruler placements fit the expected model. If the user is unhappy with the corresponding profile of a ruler, the ruler's position may be adjusted or the ruler may be deleted.

Once the user is satisfied with the set of rulers, the Estimate PSF collapsible button can be expanded, revealing a list of parameters that the user can set for PSF estimation. The default values are ideal for cortical bone structures. The user then chooses the direction (In-Plane or Out-of-Plane) of the desired PSF estimation, and

clicks the Estimate PSF button.

The estimated PSF value will be returned, and this value will cascade to the Sharpen Volume module. As well, two new plots for each intensity profile will appear in the slice view containing the original plot. The Predicted plot shows the predicted true intensities of the cortical bone, and the Fitted plot shows the Predicted plot convolved with the Gaussian (estimated PSF). The plot of the original profile and the Fitted plot should match. If they do not, then the corresponding rulers should be adjusted, and the PSF, re-estimated.



(a)

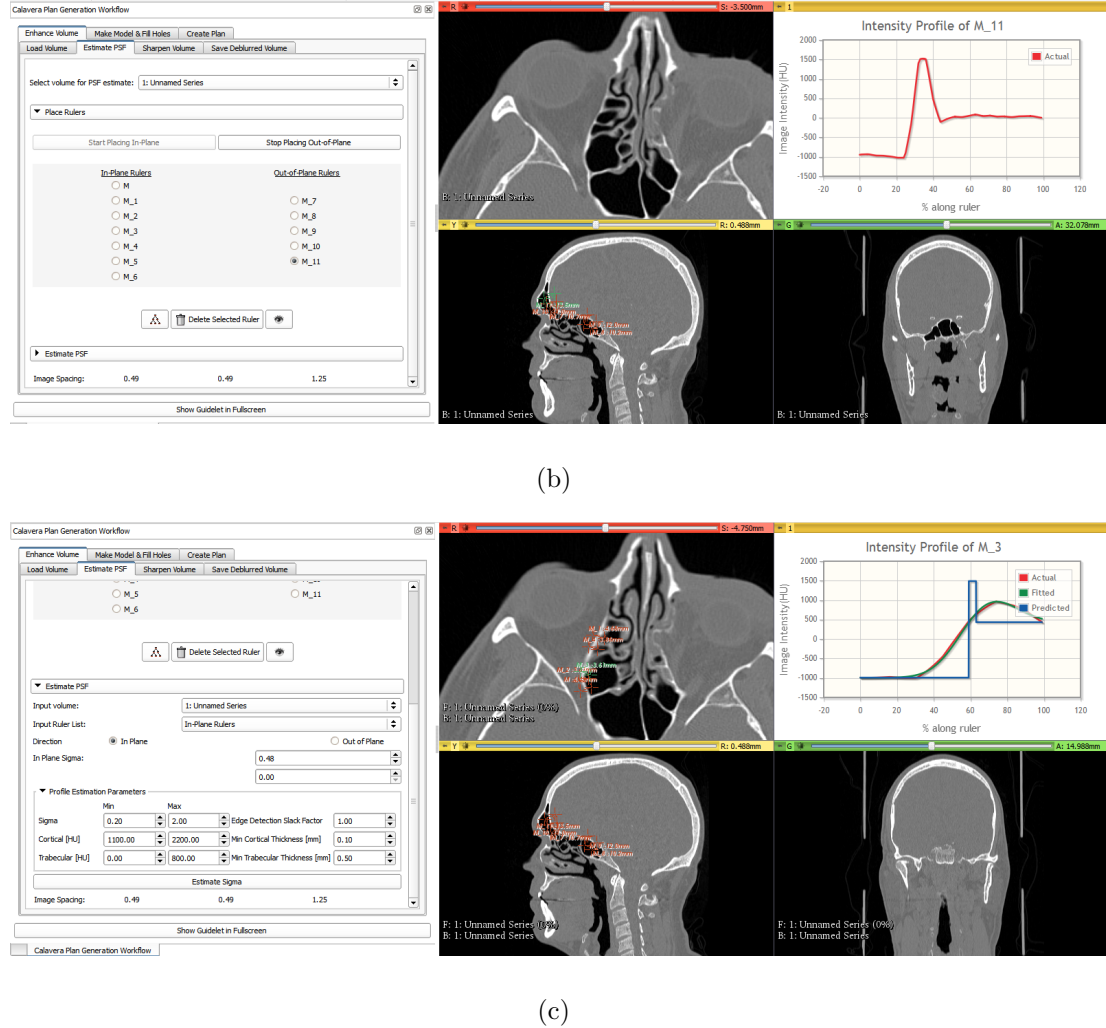


Figure 3.4: Estimate PSF module: (a) Initial state of module; (b) Rulers were placed in the scene, and the intensities associated with the highlighted green ruler can be seen plotted in the quantitative scene view (top-right quadrant); (c) The In-Plane PSF was estimated, generating two new plots in the quantitative view (where the blue plot displays the predicted intensities and the green plot displays the estimated PSF convolved with the predicted intensities).

Sharpen Volume

The Sharpen Volume module (Figure 3.5) allows the user to sharpen a volume by applying Richardson-Lucy Deconvolution or unsharp masking. The user first selects a volume to sharpen. This will default to the input volume of the Estimate PSF module. Next, the user must select the desired sharpening method(s).

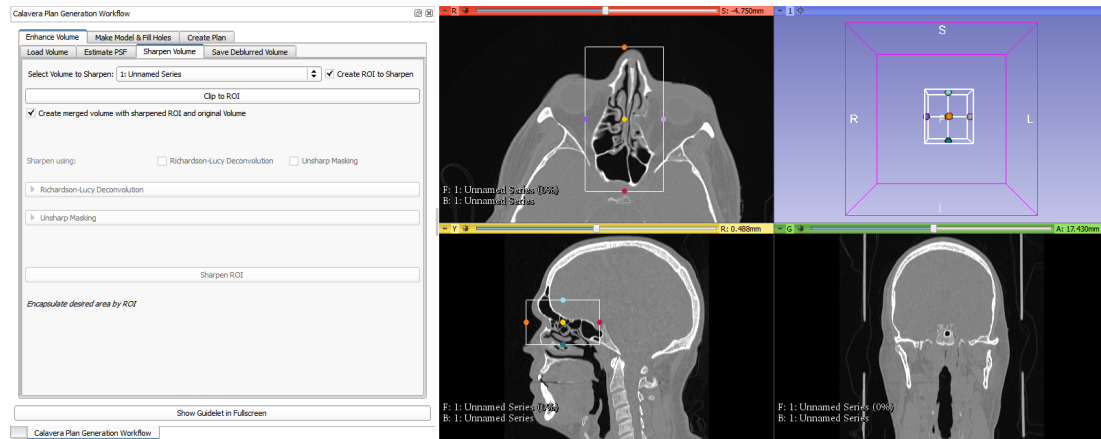
Richardson-Lucy Deconvolution requires values for In-Plane sigma and Out-of-Plane sigma, and requires the user to choose a number of iterations for which to run the algorithm, as well as the number of decimal places to be used in the PSF. If sigma values were estimated in the previous module, Estimate PSF, these will populate the fields of the current module. The preset default values for number of iterations and decimal places in the PSF reflect the optimal parameters discussed in Pakdel *et al*'s study [18]. These yielded the highest restoration of bone geometry.

Unsharp Masking requires the user to choose values for the Gaussian radius, Gaussian variance, and mask sharpness. The preset default values for these parameters reflect the optimal parameters discussed in Harada *et al*'s study [8]. These yielded the most desirable sharpening effects on thin bone structures in CTs.

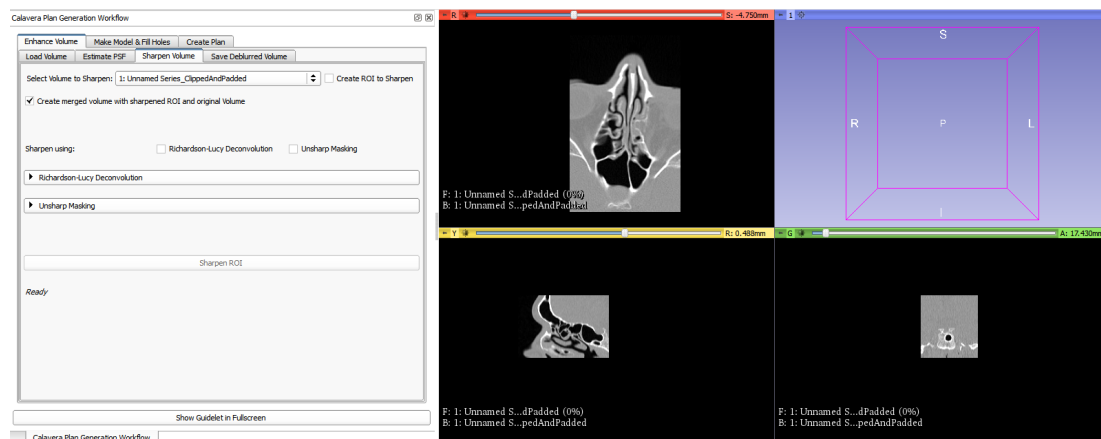
Before applying the sharpening method, the user can choose to limit the sharpening region of the volume to a region of interest (ROI), and have that sharpened ROI be merged with the original unsharpened region of the volume. Sharpening an ROI instead of the entire volume is faster, and it eliminates the possibility of raising the intensity values of undesirable areas of the volume (e.g., the patient's skin or noise artifacts present in the scan). The output of this module is a new vtkScalarVolumeNode which is sharpened.

3.2. SOFTWARE IMPLEMENTATION

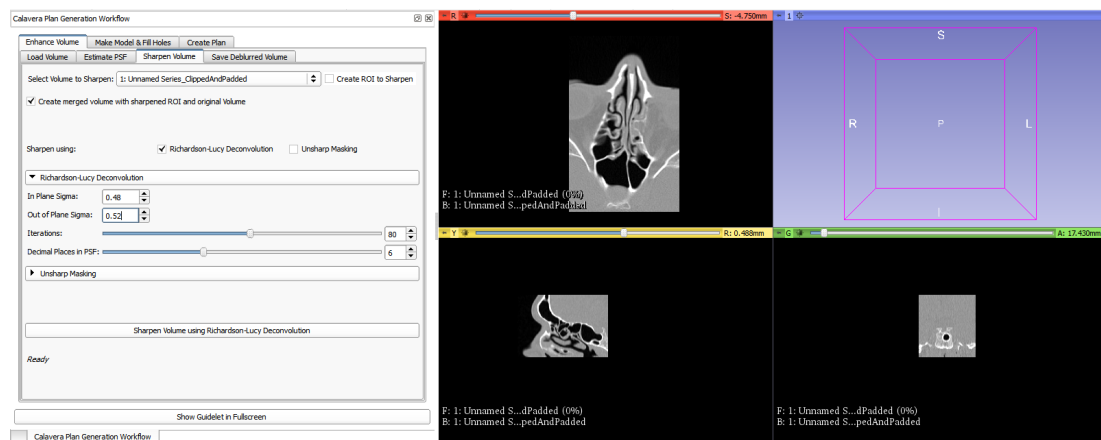
32



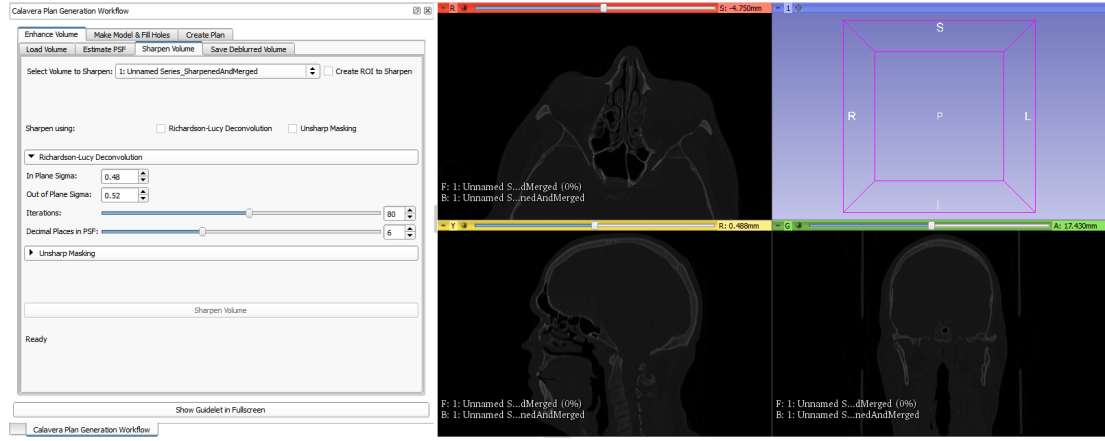
(a)



(b)



(c)



(d)

Figure 3.5: Sharpen Volume module: (a) An ROI was placed around the desired regions to sharpen: the orbital and sinal cavity; (b) The volume was clipped down to the ROI; (c) Richardson-Lucy Deconvolution was selected as the sharpening method; (d) The sharpened ROI was merged with the remainder of the original volume.

Save Deblurred Volume

The Save Deblurred Volume module (Figure 3.6) allows the user to export the sharpened volume with the original volume’s metadata. The user must select the volume to export and the DICOM volume from which to pull the metadata. Using the volume’s ID, its metadata is read from the dictionary created in the Load Volume module, and the same metadata is written to the volume to be exported. The user then selects the directory in which to export the sharpened DICOM, and proceeds to click the Export Volume to DICOM button.

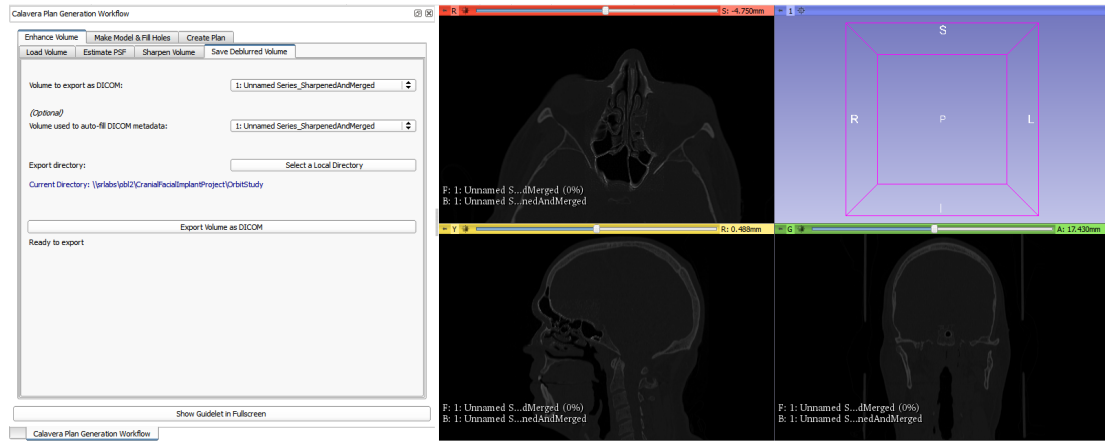


Figure 3.6: Save Deblurred Volume module: The sharpened volume exported to a local directory with the input volume’s metadata.

3.2.2 Make Model & Fill Holes

The *Make Model & Fill Holes* category is the second of the primary categories in the workflow. It enables the user to segment bone from the CT data, enhance the connectivity of the thresholded data, create a surface model, and enhance the quality of the surface model.

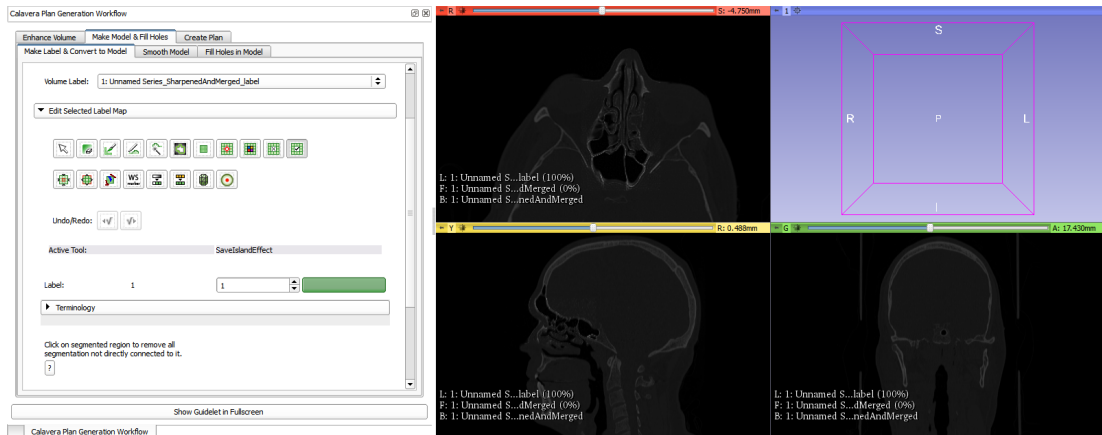
Make Label & Convert to Model

The Make Label & Convert to Model module (Figure 3.7) allows the user to go from a volume to a surface model. It incorporates 3D Slicer’s built-in Editor module and two CLIs: SegPostprocess and Model Maker.

The user begins by selecting the Input Volume. A label map will automatically be created and selected for that volume, where a label map, `vtkLabelVolumeNode`, stores only binary volume information. The user will then threshold the input volume, preserving voxels with a minimum of at least 300 Hounsfield Units (the standard

threshold for bone) and a maximum up to the volume's highest intensity value, inclusive. The label map reflects this by displaying a vtkLabelVolumeNode where voxels with intensity values equal to or greater than 300 are translated to an intensity of 1, and voxels with values less than 300 are translated to an intensity of 0.

Next, the user inputs a model name and clicks the Make Model button. Before the label map is used to construct the model, a filter which enforces spherical topology and fills in internal holes is applied to it. After this step is complete, the enhanced label map is used to create a vtkMRMLModelNode.



(a)

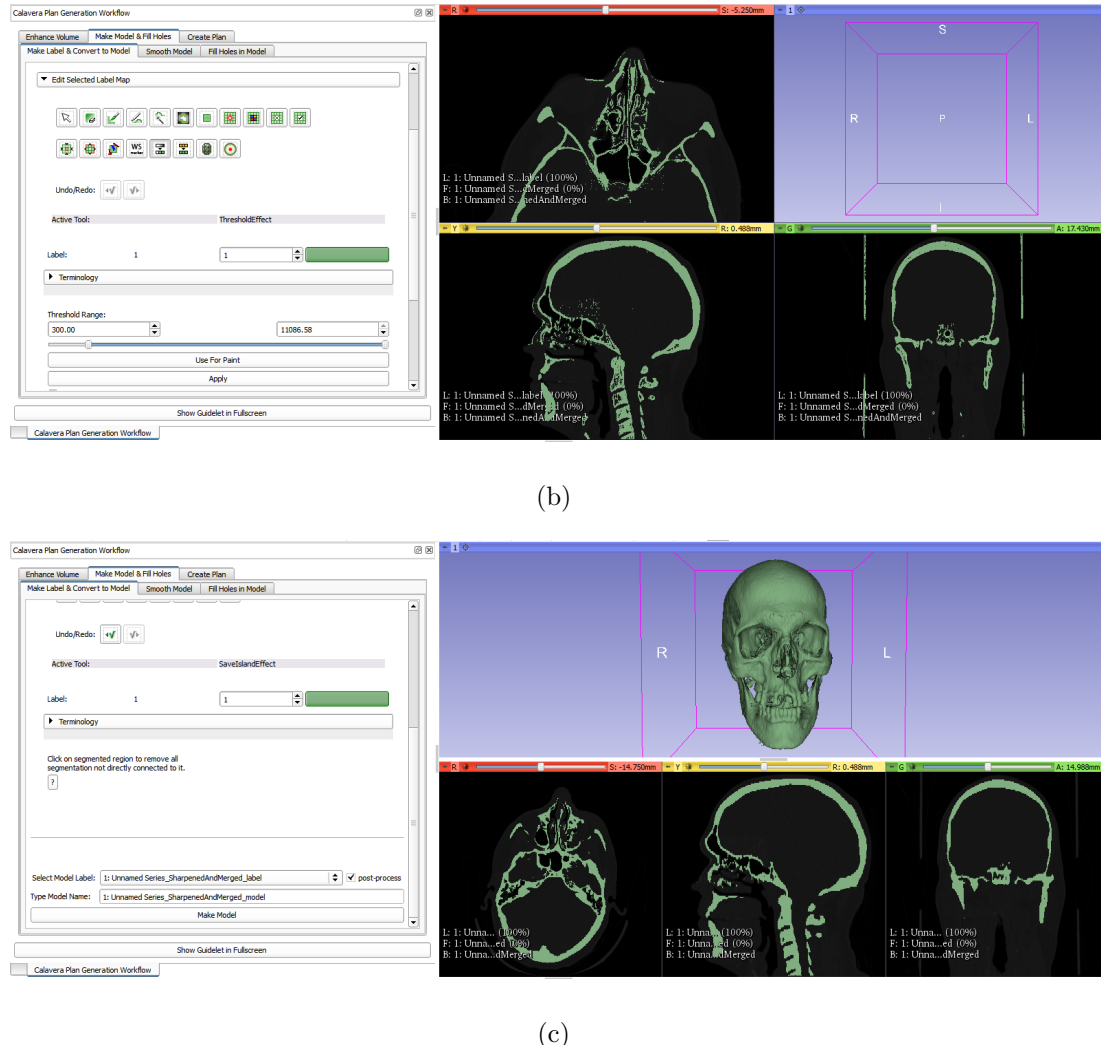


Figure 3.7: Make Label & Convert to Model module: (a) A label was created for the volume; (b) The volume was thresholded, populating the label (green); (c) Post-process was checked to apply the spherical topology enforcing filter to the label, and then a model was reconstructed using the label.

Smooth Model

The Smooth Model module (Figure 3.8) allows the user to apply a two-step smoothing filter to the model. The user must choose an input model (which defaults to the model generated from the Make Label & Convert to Model tab) as well as an output model. The user can then set values for the parameters: Smoothing Steps, Feature Angle, Normal Angle, Normal Smoothing Steps, and Vertex Fitting Steps. The preset default values for these parameters were established empirically to yield a model with reduced noise that did not have noticeable loss in sharpness of feature edges.

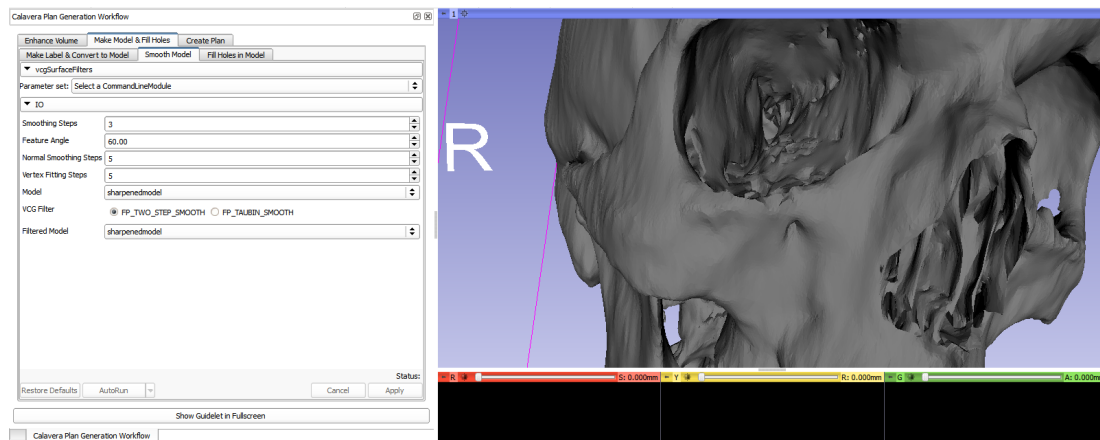


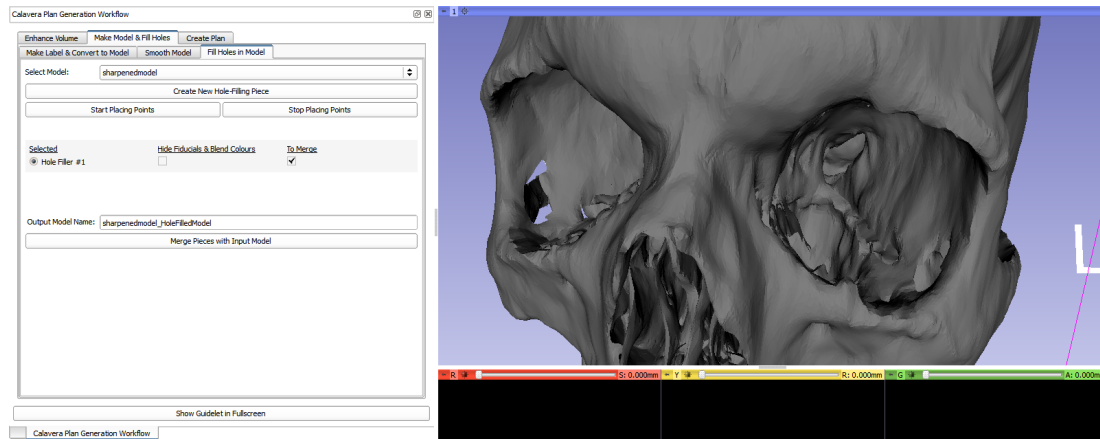
Figure 3.8: Smooth Model module: The model was smoothed using the two-step smoothing filter.

Fill Holes in Model

The Fill Holes in Model module (Figure 3.9) allows the user to create surface models which merge with the input model, ultimately filling unwanted holes. The user begins by selecting an input model (which defaults to the output model of the Smooth Model module). The user then clicks Create New Hole-Filling Piece to initialize the creation

of a hole-filling surface. Next, the user clicks Start Placing Points. This changes the mouse pointer to a fiducial-point pointer which drops a fiducial point into the scene when the mouse is clicked. The user sets down a series of fiducial points encapsulating a single hole, and then clicks Stop Placing Points. When the Hide Fiducials and Blend Colours checkbox is pressed, these points are used to form hole-covering surfaces.

The algorithm used first relocates the user-placed points by snapping them to the nearest point on the input model. Next, these points are used in 3D Delaunay triangulation to form a convex surface. The generated convex hull is a surface model made up of polygonal faces, and is not a filled tetrahedral mesh. This surface is then deformably registered to the input model, creating a hole-filling piece with curvature that fits the curvature of the surface around the hole's parameter. The user creates a new hole-filling piece for each hole that should be closed. Then, the user clicks Merge Pieces with Input Model to generate an output model that combines data points from the original model and all the hole-filling pieces. The polydata from all the surface models is merged, and is used to create a new surface model.



(a)

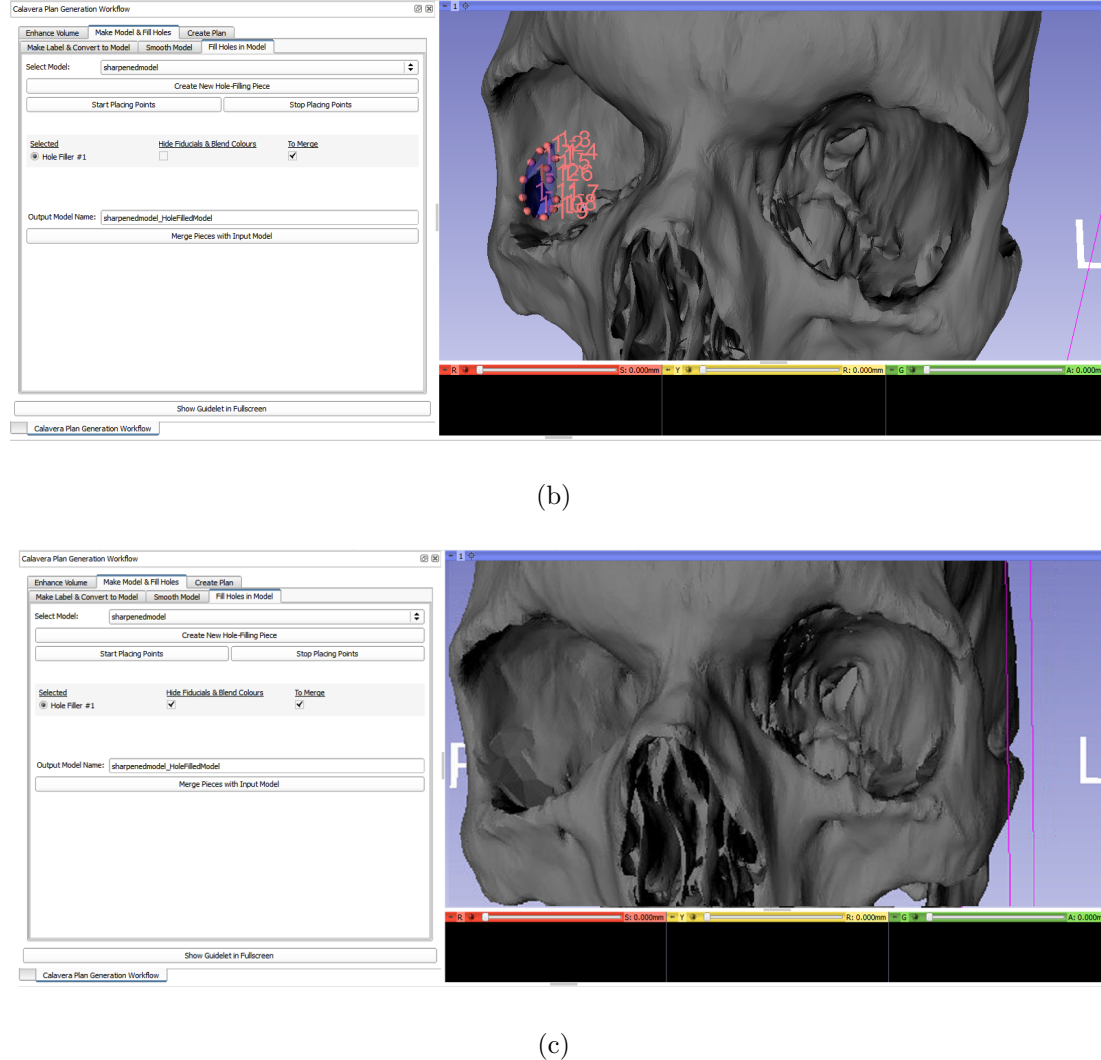


Figure 3.9: Fill Holes in Model module: (a) Hole-filling piece was initialized; (b) Fiducial points were placed around hole; (c) Hole-filling piece was created, and fiducial points were hidden by ticking appropriate checkbox.

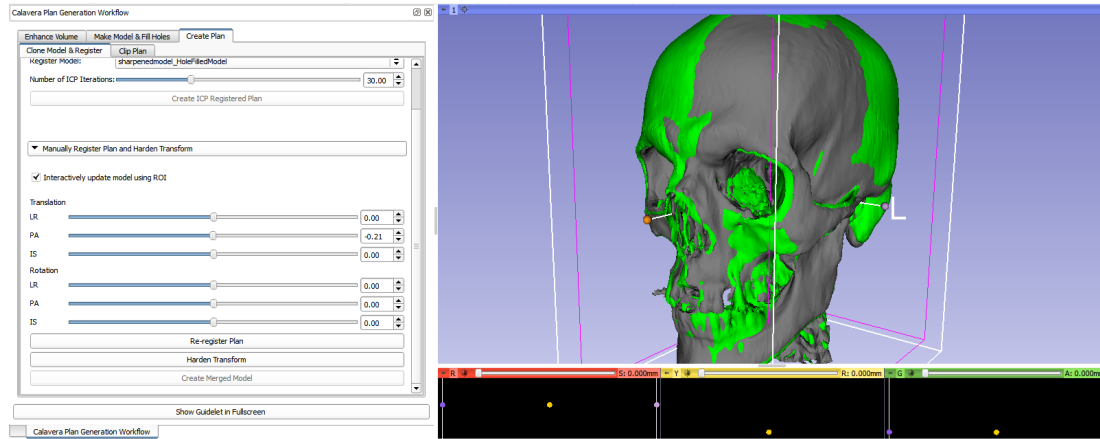
3.2.3 Create Plan

The *Create Plan* category is the third of the primary tabs in the workflow. It enables the user to create an implant plan, and export the plan outside the 3D Slicer

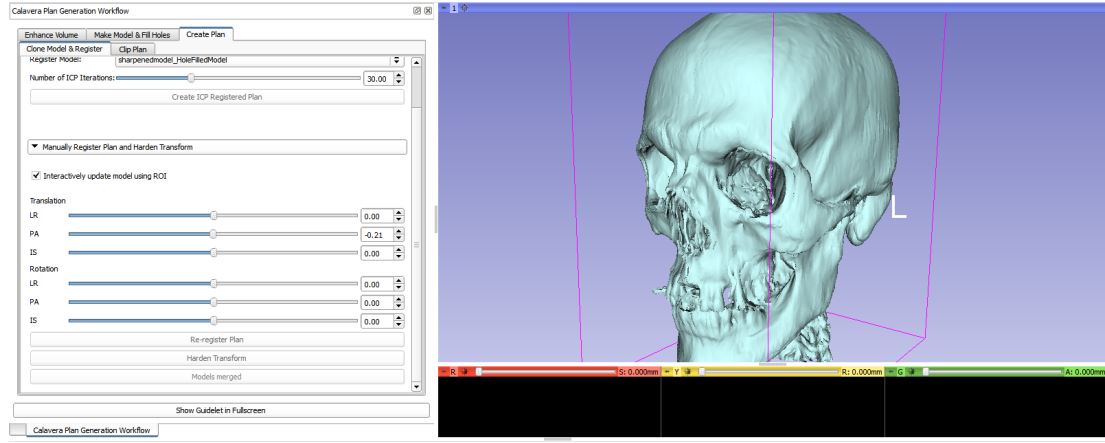
environment.

Clone Model & Register

The Clone Model & Register module (Figure 3.10) allows the user to register the damaged side of the skull with the contralateral, healthy side. The user begins by selecting an input model (which defaults to the output of the Fill Holes in Model module). Then the number of ICP iterations is selected, and the user clicks Create ICP Registered Plan. This creates a clone of the input model that is mirrored and registered to the original. Once ICP registration is complete, the user is able to manually translate the cloned model by interactively dragging the edges of the ROI or by moving the sliders. The sliders can also be used to rotate the model. After manually transforming the cloned model, the user can choose to re-register it using ICP registration. Once satisfied with the registration, the user clicks the Harden Transform and the Create Merged Model buttons to lock the cloned model's new position, and create a model that merges the data of both the original model and the cloned model, respectively.



(a)



(b)

Figure 3.10: (a) Clone Model & Register module: (a) Create ICP Registered Plan button was pressed, creating a mirrored, registered model (green) of the original (grey); (b) The geometry of both models was merged and used to create a new model (white).

Clip Plan

The Clip Plan module (Figure 3.11) allows the user to crop the hole-filled, restored model to the desired plan area. The user begins by selecting the input model to clip. Then the user clicks Start Clipping Model which creates an ROI that encapsulates the model. The user then drags the edges of the ROI to the desired plan area, causing the model size to update accordingly. Once the user is satisfied with the plan, the user clicks Keep & Name Clipped Model.

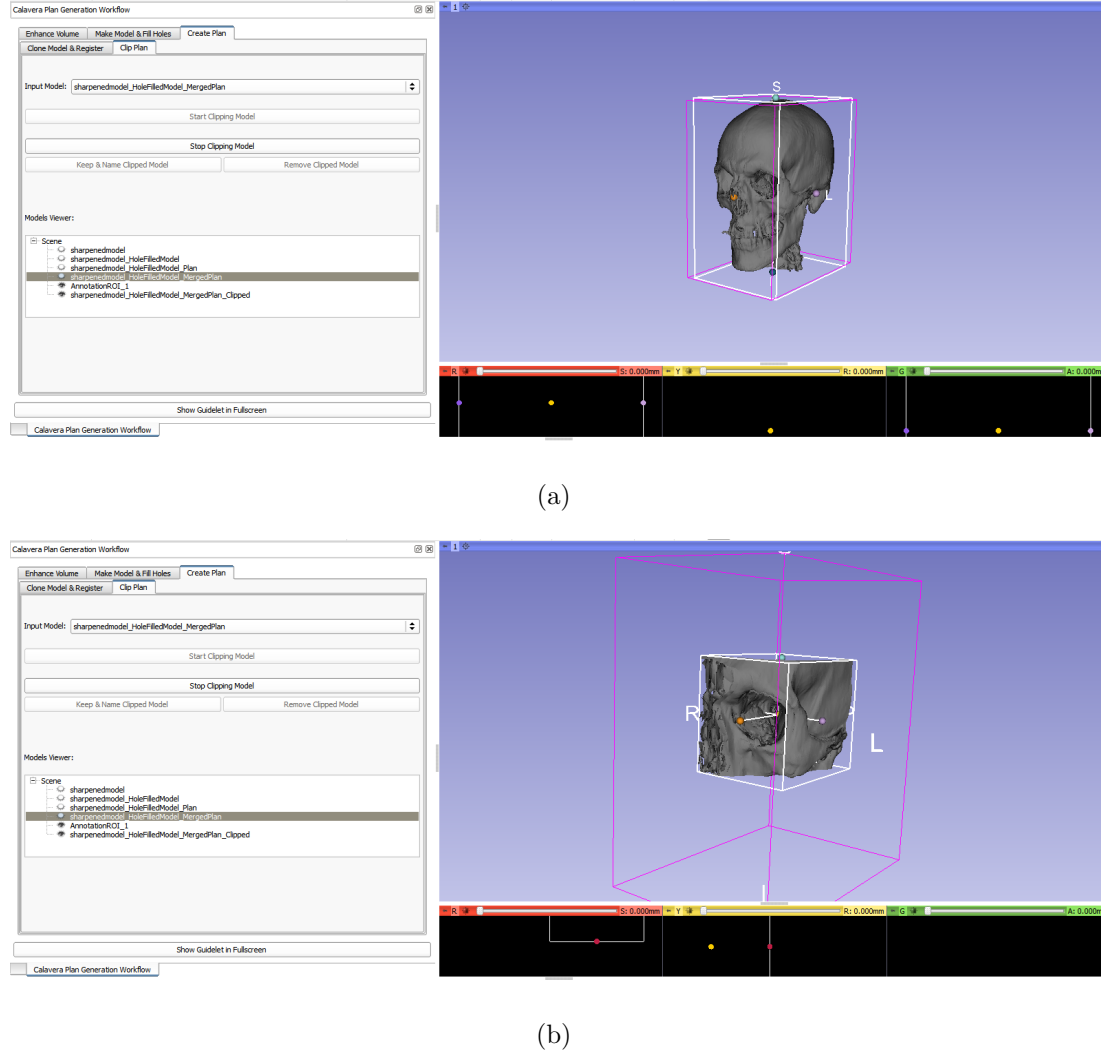


Figure 3.11: Clip Plan module: (a) An ROI encapsulates the selected model; (b) The model was clipped to the desired area by resizing the ROI.

3D Slicer allows the user to export all models necessary for plan creation to a local directory. The user clicks the Save Data button, causing a window to appear that prompts the user to select the models to be exported, as well as the data type and location to which they should be exported.

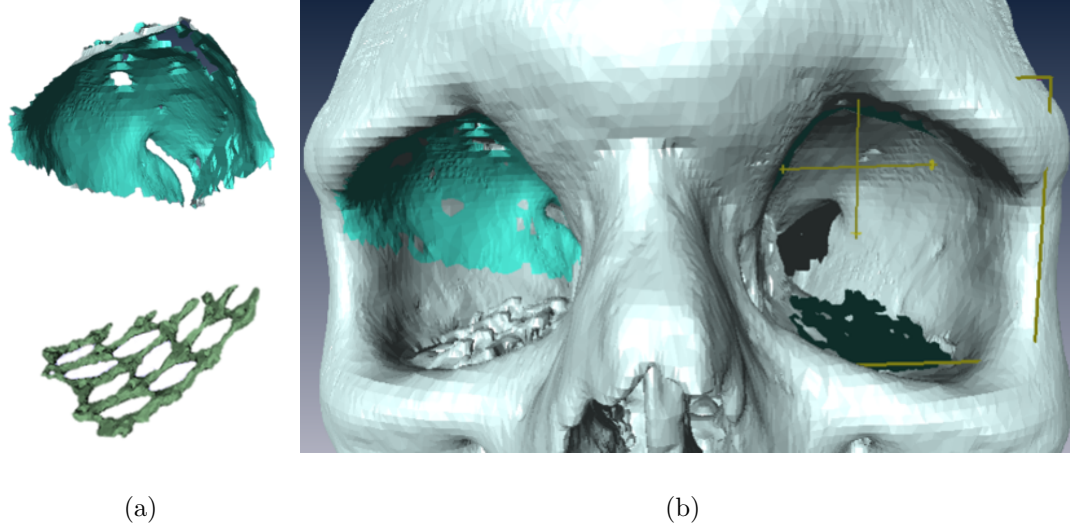
3.3 Software Application Study

To carry out this study, ethics approval was obtained that granted access to the post-operative CT scans of 13 patients on whom orbital reconstruction surgery was performed by expert surgeons from the Calavera Surgical™ team. Restored skull models were generated using the CT data of these 13 patients. Four of these patients had implants that were pre-operatively designed by the Calavera Surgical™ technician using the manual-segmentation approach. The other 9 patients had implants that were hand-designed intra-operatively by the two expert surgeons on the Calavera Surgical™ team. Implants for all 13 patients were implanted by these two surgeons. A morphological analysis was carried out to assess the accuracy and time-efficiency of our software in generating skull models for use in implant design. This analysis was carried out using AMIRA (AMIRA, Mercury Computer Systems, Berlin, Germany), a software for medical image visualization and analysis.

First, an analysis on restored orbital symmetry was carried out to assess the accuracy of the CAD implants designed by Calavera Surgical™ compared against reconstruction using implants hand-shaped by two expert surgeons on the Calavera Surgical™ team. Greater symmetry between a pair of orbits translates to improved aesthetic outcome and a greater chance of treating enophthalmos and diplopia [15].

The degree of orbital symmetry was calculated by comparing the distance between the implant's surface and the equivalent surface of the contralateral side. First, a post-operative CT scan of the patient was used to segment the implant and the bone from the CT data. Then the implant segmentation and the bone segmentation were used to reconstruct 3D models of the implant and skull, respectively. Using the skull model, the undamaged portion of the orbit containing the implant was extracted,

copied, and saved as a separate model. The undamaged surface model was then mirrored and registered to the contralateral, healthy orbit. The transformation used to carry out the mirroring and registration of the undamaged surface model was applied to the implant model as well. The distance between the undamaged orbital floor and the implant model was measured, and was recorded under *Morphological Analysis: Implant vs Contralateral Orbit (Unregistered)*. This method gives only an approximation to the level of restored symmetry between the orbits. It assumes the roofs of a pair of orbits to be perfectly symmetrical, which they are not in practice. To get a sense of the symmetry in shape between the two orbits, the implant model was then registered to the skull surface. The distance between the undamaged orbital floor and the implant model was measured, and was recorded under *Morphological Analysis: Implant vs Contralateral Orbit (Registered to Orbital Floor)*.



(a)

(b)

Figure 3.12: (a) Segmented undamaged region of the right orbit (blue) and segmented implant (green); (b) Skull model in which the right undamaged region was registered to the left undamaged region, and the implant from the right orbit was registered to the healthy surface of the left orbit.

The software presented in this thesis was then compared against the manual segmentation method previously used by Calavera SurgicalTM. To assess the similarity in shape, the healthy regions from the models generated by Calavera SurgicalTM and those generated using our software were compared. The undamaged region from our software was segmented, and the distance from it to the Calavera SurgicalTM model was measured and recorded under *Our Software Undamaged Orbit vs Calavera Undamaged Orbit*.

To determine the distance between surfaces pairs, the mean of the distances between the vertices of one surface and the nearest point on the second surface, for each vertex, was calculated.

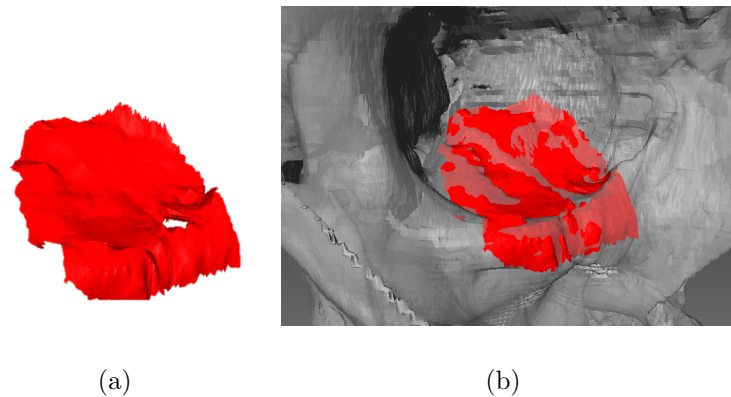


Figure 3.13: (a) Segmented surface model of the healthy orbit created using our software; (b) Skull model created using Calavera Surgical's™ existing methods overlaid by the segmented surface model created using our software.

Chapter 4

Results and Discussion

4.1 Results

Measurements carried out on patient data demonstrate that the orbits reconstructed using Calavera Surgical's™ method result in no noticeable visible difference in orbital symmetry compared to hand-shaped implants (Table 4.1). In patients where implants were designed by Calavera Surgical™ (cases), the average difference in orbital symmetry was found to be $1.3 \text{ mm} \pm 0.61 \text{ STD}$ prior to registration to the orbital surface, and $0.6 \text{ mm} \pm 0.17 \text{ STD}$ after registration. In patients where implants were hand-shaped by expert surgeons intra-operatively (controls), the average difference in orbital symmetry was found to be $1.5 \text{ mm} \pm 0.80 \text{ STD}$ prior to registration to the orbital surface, and $0.8 \text{ mm} \pm 0.14 \text{ STD}$ after registration. These results can be seen in Table 4.2. Although the outcomes appear similar between the two groups, given the small sample size of patient data ($n=13$), no significant result can be concluded since the outcome of carrying out an independent groups t-test had a p-value of 0.39 and 0.10 for the unregistered and registered groups, respectively (where a p-value less than 0.05 is considered significant).

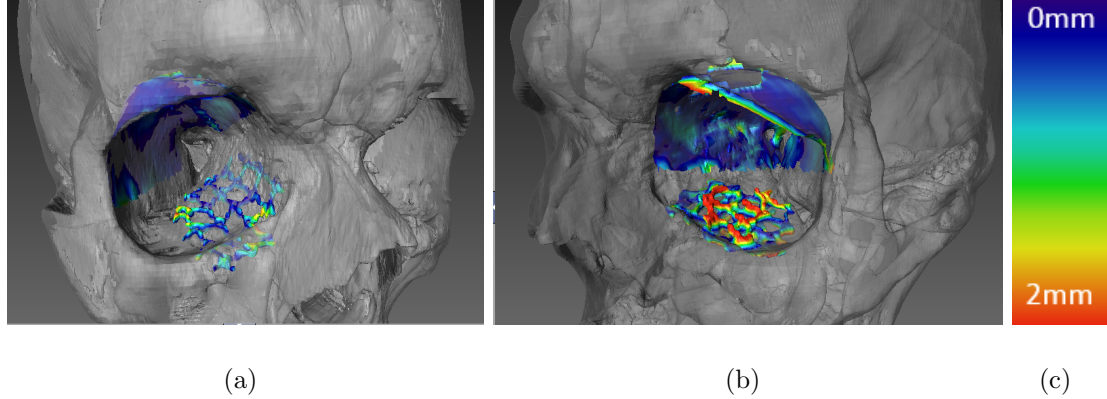
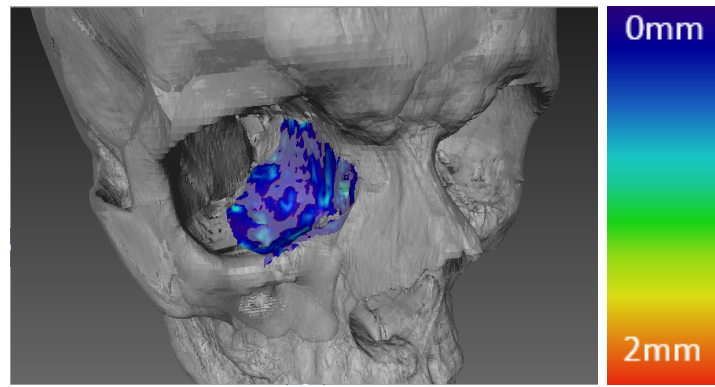


Figure 4.1: Post-operative patient skull models displaying distance between implant model and contralateral healthy orbit, where the implant was designed by (a) Calavera Surgical'sTM existing methods and (b) hand-shaping; (c) Distance colour-map.

The skull models generated by our software were similar to those generated by using Calavera Surgical'sTM manual segmentation method. The difference in distance between the surface pairs was found to be $0.4 \text{ mm} \pm 0.17 \text{ STD}$, on average (Table 4.4).

Using our software to design implant plans took a much shorter period of time compared to that reported by Calavers SurgicalTM. Design time using Calavera Surgical'sTM existing manual segmentation methods was reported to be between 3 and 6 hours, whereas our software design time ranged between between 0.25 and 0.42 hours, with an average of $0.33 \text{ hours} \pm 0.04 \text{ STD}$. There was no measurable trend between the CT pixel size and the design time for processing such CTs (Table 4.3).



(b)

Figure 4.2: (a) Undamaged orbit model of patient generated using our software (blue) against skull model generated using Calavera Surgical'sTM current method; (b) Distance colour-map.

Table 4.1: Morphological Analysis: Implant vs Contralateral Orbit

Patient Type	Patient Number	Registered to Orbital Floor (mm)	Unregistered (mm)
Case	1	0.4	0.6
	2	0.6	1.3
	3	0.8	1.3
	4	0.7	2.1
Control	5	0.8	1.4
	6	0.8	3.3
	7	0.9	1.2
	8	0.8	1.9
	9	0.7	1.3
	10	1.1	1.6
	11	0.8	0.6
	12	0.6	0.9
	13	0.7	0.9

Table 4.2: Morphological Analysis: Implant vs Contralateral Orbit (Statistics)

Measure	Registered To Orbital Floor	Unregistered
Mean	Case: 0.6 mm \pm 0.17 STD	Case: 1.3 mm \pm 0.61 STD
	Control: 0.8 mm \pm 0.14 STD	Control: 1.5 mm \pm 0.80 STD

Table 4.3: Morphological Analysis: Design Using Our Software

Patient Number	CT Spacing LengthxWidthxDepth (mm)	Design Time (hours)	Our Software vs Manually-Segmented Undamaged Orbit (mm)
1	0.49x0.49x0.63	0.42	0.2
2	0.49x0.49x1.25	0.35	0.3
3	0.49x0.49x1.25	0.25	0.3
4	0.35x0.35x1.25	0.30	0.5
5	0.49x0.49x1.25	0.34	0.2
6	0.49x0.49x1.25	0.33	0.4
7	0.49x0.49x1.25	0.35	0.3
8	0.49x0.49x1.25	0.25	0.8
9	0.49x0.49x1.25	0.35	0.5
10	0.59x0.59x1.25	0.35	0.5
11	0.35x0.35x0.63	0.34	0.4
12	0.49x0.49x1.25	0.35	0.4
13	0.49x0.49x1.25	0.32	0.5

Table 4.4: Morphological Analysis: Design Using Our Software (Statistics)

Measure	Design Time	Our Software vs Manually-Segmented Undamaged Orbit
Mean	0.33 hours \pm 0.04 STD	0.4 mm \pm 0.17 STD

4.2 Discussion

It is difficult to assess the accuracy in the differences between implants designed using Calavera Surgical's™ existing methods and those that are hand-shaped since the average measurement differences found were on a sub-millimeter scale, which is similar to the scale of the image resolution of CT scans. Another area that could have skewed the results is the distance measure used in assessing symmetry. The method used looked at all the vertices of the implant and matched those to the nearest points on the orbital surface. Only the vertices on the top surface of the implant characterize symmetry, so only those vertices should be matched. Moreover, the undamaged regions of the orbital roofs are used to assess orbital symmetry (prior to registration), but there have been no studies in the literature that discuss how symmetric they are, themselves.

One of the primary focuses and advantages of utilizing Calavera Surgical's™ custom implants was the reduction of intra-operative surgical time. Increasing the sample size with incoming cases will determine the significance of the results. In the meantime, monitoring of patients with Calavera Surgical™ implants will continue.

Chapter 5

Conclusions and Future Work

5.1 Conclusions

The goal of this thesis was to create software for the efficient and accurate design of orbital-craniofacial implants, with a focus on decreasing design time compared to current CAD methods. Methods for improving medical image quality as well as surface quality have been researched and implemented within our software developed using the Slicer platform. Our software has been used to reconstruct skull models for 13 patients, and it has produced models similar in geometry to those reconstructed using Calavera Surgical'sTM existing methods. Moreover, user design time has been thoroughly decreased.

5.2 Future Work

The current software presents many avenues for future work. One fundamental feature that should be implemented within Slicer is a module for smoothing the merged model composed of the original and registered, mirrored version. As it currently stands, this step is carried out outside the Slicer workflow.

Moreover, the existing Calavera Surgical™ software and our software need to be tested in a greater number of reconstruction cases to demonstrate an ability to restore orbital symmetry effectively in a statistically significant way.

Bibliography

- [1] Z. Al-Ameen, G. Sulong, and G. Johar. Reducing the Gaussian blur artifact from CT medical images by employing a combination of sharpening filters and iterative deblurring algorithms. *Journal of Theoretical and Applied Information Technology*, 46(1):31–36, 2012.
- [2] P. J. Besl and N. D. McKay. A Method for Registration of 3-D Shapes, *IEEE Transactions on Pattern Analysis and Machine Intelligence*, 14(2): 239–256, 1992.
- [3] Z. Bian and R. Tong. Feature-preserving mesh denoising based on vertices classification. *Computer Aided Geometric Design*, 28(1):50–64, 2011.
- [4] A. Bowyer. Computing Dirichlet tessellations. *The Computer Journal*, 24(2):162–166, 1981.
- [5] C. Cornelius, N. Gellrich, S. Hillerup, K. Kusumoto, W. Schubert, S. Fusetti, E. Barth, and H. Essig. AO Surgery Reference, 2009.
- [6] G. Dougherty and D. Newman. Measurement of thickness and density of thin structures by computed tomography: a simulation study. *Medical Physics*, 26(7):1341–1348, 1999.

- [7] P. S. D'Urso, W. J. Earwaker, T. M. Barker, M. J. Redmond, R. G. Thompson, D. J. Effeney, and F. H Tomlinson. Custom cranioplasty using stereolithography and acrylic. *British Journal of Plastic Surgery*, 53:200–204, 2000.
- [8] T. Harada, K. Nishikawa, and K. Kuroyanagi. Unsharp masking technique as a preprocessing filter for improvement of 3D-CT image of bony structure in the maxillofacial region. *Oral Radiology*, 14(2):85–94, 1998.
- [9] B. Jian and B. C. Vemuri. A Robust Algorithm for Point Set Registration Using Mixture of Gaussians. *Proceedings of the Tenth IEEE International Conference on Computer Vision*, 10:1246–1251, 2005.
- [10] S. Johnson, J. Joannopoulos, and M. Soljačić. The NLopt nonlinear-optimization package.
- [11] W.A. Kalender. Computed Tomography: Fundamentals, System Technology, Image Quality, Applications. Wiley, 2011.
- [12] H. Karim, D. Wijetunge, S. Grubnic, and I. Jackson. A Comprehensive Analysis of Craniofacial Trauma. *Journal of Trauma*, 36(1):34-47, 1994.
- [13] M. Kozakiewicz, M. Elgalal, P. Loba, P. Komuński, P. Arkuszewski, A. Broniarczyk-Loba, and L. Stefańczyk. Clinical application of 3D pre-bent titanium implants for orbital floor fractures. *Journal of Cranio-Maxillofacial Surgery*, 37(4):229–234, 2009.
- [14] W. Z. Li, M. C. Zhang, S. P. Li, L. T. Zhang, and Y. Huang. Application of computer-aided three-dimensional skull model with rapid prototyping technique

- in repair of zygomatico-orbito-maxillary complex fracture. *The International Journal of Medical Robotics and Computer Assisted Surgery*, 5:158–163, 2009.
- [15] O. Lieger, R. Richards, M. Liu, and T. Lloyd. Computer-assisted design and manufacture of implants in the late reconstruction of extensive orbital fractures. *Archives of facial plastic surgery : official publication for the American Academy of Facial Plastic and Reconstructive Surgery*, 12(3):186–191, 2010.
- [16] W. E. Lorensen and H. E. Cline. Marching cubes: A high resolution 3D surface construction algorithm. *Computer Graphics*, 21(4):163–169, 1987.
- [17] J. G. Mainprize, G. Edwards, and O. Antonyshyn. Project Proposal for OCE. Technical report, 2013.
- [18] A. Pakdel, M. Hardisty, J. Fialkov, and C. Whyne. Restoration of Thickness, Density, and Volume for Highly Blurred Thin Cortical Bones in Clinical CT Images. *Annals of Biomedical Engineering*, 2016.
- [19] A. Pakdel, J. G. Mainprize, N. Robert, J. Fialkov, and C. M. Whyne. Model-based PSF and MTF estimation and validation from skeletal clinical CT images. *The International Journal of Medical Physics Research and Practice*, 41(1), 2014.
- [20] J. Parthasarathy. 3D modeling, custom implants and its future perspectives in craniofacial surgery. *Annals of Maxillofacial Surgery*, 4(1):9, 2014.
- [21] A. M. Pham, A. A. Rafii, M. C. Metzger, A. Jamali, and E. B. Strong. Computer modeling and intraoperative navigation in maxillofacial surgery. *Otolaryngology-Head and Neck Surgery*, 137:624–631, 2007.

- [22] J. Schipper, G. J. Ridder, U. Spetzger, C. B. Teszler, M. Fradis, and W. Maier. Individual prefabricated titanium implants and titanium mesh in skull base reconstructive surgery. A report of cases. *European Archives of Otorhinolaryngology*, 261(5):282–290, 2004.
- [23] S. Singare, L. Dichen, L. Bingheng, G. Zhenyu, and L. Yaxiong. Customized design and manufacturing of chin implant based on rapid prototyping. *Rapid Prototyping Journal*, 11(2):113–118, 2005.
- [24] M. Styner, I. Oguz, S. Xu, C. Brechbühler, D. Pantazis, J. J. Levitt, M. E. Shenton, and G. Gerig. Framework for the Statistical Shape Analysis of Brain Structures using SPHARM-PDM. *The Insight Journal*, 1071:242–250, 2006.
- [25] M. Temerinac-Ott. Tile-based Lucy-Richardson Deconvolution Modelling a Spatially-Varying PSF for Fast Multiview Fusion of Microscopical Images. Technical Report 260, 2010.
- [26] G. M. Treece, A. H. Gee, P. M. Mayhew, and K. E S Poole. High resolution cortical bone thickness measurement from clinical CT data. *Medical Image Analysis*, 14(3):276–290, 2010.
- [27] C. S. Varnan, A. Jagan, J. Kaur, D. Jyoti, and D. S. Rao. Image Quality Assessment Techniques in Spatial Domain. *International Journal of Computer Science and Technology*, 2(3):177–184, 2011.

Appendix A

12/12/2016

RightsLink Printable License

**ELSEVIER LICENSE
TERMS AND CONDITIONS**

Dec 12, 2016

This Agreement between Amani Ibrahim ("You") and Elsevier ("Elsevier") consists of your license details and the terms and conditions provided by Elsevier and Copyright Clearance Center.

License Number	4006540180222
License date	Dec 12, 2016
Licensed Content Publisher	Elsevier
Licensed Content Publication	Computer Aided Geometric Design
Licensed Content Title	Feature-preserving mesh denoising based on vertices classification
Licensed Content Author	Zhe Bian,Ruofeng Tong
Licensed Content Date	January 2011
Licensed Content Volume Number	28
Licensed Content Issue Number	1
Licensed Content Pages	15
Start Page	50
End Page	64
Type of Use	reuse in a thesis/dissertation
Intended publisher of new work	other
Portion	figures/tables/illustrations
Number of figures/tables/illustrations	4
Format	both print and electronic
Are you the author of this Elsevier article?	No
Will you be translating?	No
Order reference number	
Original figure numbers	Figure 13 a,b,e,f
Title of your thesis/dissertation	Software for Designing CustomOrbital-Craniofacial Implant Plans
Expected completion date	Dec 2016
Estimated size (number of pages)	60
Elsevier VAT number	GB 494 6272 12
Requestor Location	Amani Ibrahim 31 Avery Court

Richmond Hill, ON L4B3W1

12/12/2016

RightsLink Printable License

**ELSEVIER LICENSE
TERMS AND CONDITIONS**

Dec 12, 2016

This Agreement between Amani Ibrahim ("You") and Elsevier ("Elsevier") consists of your license details and the terms and conditions provided by Elsevier and Copyright Clearance Center.

License Number	4006530859818
License date	Dec 12, 2016
Licensed Content Publisher	Elsevier
Licensed Content Publication	British Journal of Plastic Surgery
Licensed Content Title	Custom cranioplasty using stereolithography and acrylic
Licensed Content Author	Paul S. D'Urso,David J. Effeney,W. John Earwaker,Timothy M. Barker,Michael J. Redmond,Robert G. Thompson,Francis H. Tomlinson
Licensed Content Date	April 2000
Licensed Content Volume Number	53
Licensed Content Issue Number	3
Licensed Content Pages	5
Start Page	200
End Page	204
Type of Use	reuse in a thesis/dissertation
Intended publisher of new work	other
Portion	figures/tables/illustrations
Number of figures/tables/illustrations	3
Format	both print and electronic
Are you the author of this Elsevier article?	No
Will you be translating?	No
Order reference number	
Original figure numbers	Figure 3, Figure 4, Figure 5
Title of your thesis/dissertation	Software for Designing Custom Orbital-Craniofacial Implant Plans
Expected completion date	Dec 2016
Estimated size (number of pages)	60
Elsevier VAT number	GB 494 6272 12
Requestor Location	Amani Ibrahim 31 Avery Court

Richmond Hill, ON L4B3W1

<https://s100.copyright.com/AppDispatchServlet>

1/6

12/13/2016

RightsLink Printable License

**ELSEVIER LICENSE
TERMS AND CONDITIONS**

Dec 13, 2016

This Agreement between Amani Ibrahim ("You") and Elsevier ("Elsevier") consists of your license details and the terms and conditions provided by Elsevier and Copyright Clearance Center.

License Number	4007120530796
License date	Dec 13, 2016
Licensed Content Publisher	Elsevier
Licensed Content Publication	Journal of Cranio-Maxillofacial Surgery
Licensed Content Title	Clinical application of 3D pre-bent titanium implants for orbital floor fractures
Licensed Content Author	Marcin Kozakiewicz,Marcin Elgalal,Piotr Loba,Piotr Komuński,Piotr Arkuszewski,Anna Broniarczyk-Loba,Ludomir Stefańczyk
Licensed Content Date	June 2009
Licensed Content Volume Number	37
Licensed Content Issue Number	4
Licensed Content Pages	6
Start Page	229
End Page	234
Type of Use	reuse in a thesis/dissertation
Portion	figures/tables/illustrations
Number of figures/tables/illustrations	2
Format	both print and electronic
Are you the author of this Elsevier article?	No
Will you be translating?	No
Order reference number	
Original figure numbers	Figure 5, Figure 6
Title of your thesis/dissertation	Software for Designing CustomOrbital-Craniofacial Implant Plans
Expected completion date	Dec 2016
Estimated size (number of pages)	60
Elsevier VAT number	GB 494 6272 12
Requestor Location	Amani Ibrahim 31 Avery Court

Richmond Hill, ON L4B3W1

12/12/2016

RightsLink Printable License

**SPRINGER LICENSE
TERMS AND CONDITIONS**

Dec 12, 2016

This Agreement between Amani Ibrahim ("You") and Springer ("Springer") consists of your license details and the terms and conditions provided by Springer and Copyright Clearance Center.

License Number	4006540545020
License date	Dec 12, 2016
Licensed Content Publisher	Springer
Licensed Content Publication	Annals of Biomedical Engineering
Licensed Content Title	Restoration of Thickness, Density, and Volume for Highly Blurred Thin Cortical Bones in Clinical CT Images
Licensed Content Author	Amirreza Pakdel
Licensed Content Date	Jan 1, 2016
Licensed Content Volume Number	44
Licensed Content Issue Number	11
Type of Use	Thesis/Dissertation
Portion	Figures/tables/illustrations
Number of figures/tables/illustrations	1
Author of this Springer article	No
Order reference number	
Original figure numbers	Figure 5
Title of your thesis / dissertation	Software for Designing CustomOrbital-Craniofacial Implant Plans
Expected completion date	Dec 2016
Estimated size(pages)	60
Requestor Location	Amani Ibrahim 31 Avery Court Richmond Hill, ON L4B3W1 Canada Attn: Amani Ibrahim
Billing Type	Invoice
Billing Address	Amani Ibrahim 31 Avery Court Richmond Hill, ON L4B3W1 Canada Attn: Amani Ibrahim
Total	0.00 USD



AMERICAN ASSOCIATION
of PHYSICISTS IN MEDICINE

Angela R. Keyser
Executive Director
akeyser@aapm.org
571.298.1285

DATE OF REQUEST: December 12/ 2016

FROM:

Amani Ibrahim, 31 Avery Court, Richmond Hill, ON, Canada, L4B 3W1

EMAIL ADDRESS: 9ai15@queensu.ca

1. Permission is granted to:

Amani Ibrahim, Queen's University

2. Permission is requested to use the following material:

Figure 2 of A. Pakdel, J. G. Mainprize, N. Robert, J. Fialkov, and C. M. Whyne. Modelbased PSF and MTF estimation and validation from skeletal clinical CT images. The Internal Journal of Medical Physics Research and Practice, 41(1), 2014.

3. For what purpose:

Electronic and hard copy of MSc Thesis: Software for Designing Custom Orbital-Craniofacial Implant Plans

Authors seeking permission must also notify the first author of the article from which permission is being sought.

Permission is hereby granted:

Signature

12/13/16

Date

Submit via Email

Reset Form

The Association's Journals are Medical Physics and Journal of Applied Medical Physics
Member Society of the American Institute of Physics and the International Organization of Medical Physics